Highly Selective and Reusable Porphyrin-Functionalized MCM-41 for Efficient Lead(II) Removal from Contaminated Water: Comprehensive Adsorption Study and Real-Water Validation

Youssef Draoui[1,2], Smaail Radi[2,*], Mengmeng Wang[1], Amal El Mahdaoui[2], Chahrazad El Abiad,[2] Aurelian Rotaru[4], Yann Garcia[2]*, M. Amparo F. Faustino[3], M. Graça P. M. S. Neves[3], Nuno M. M. Moura[3,*]

[1] *Institute of Condensed Matter and Nanosciences, Molecular Chemistry, Materials and Catalysis (IMCN/MOST), Université Catholique de Louvain, Place L. Pasteur 1, 1348 Louvain-la-Neuve, Belgium.*

[2] *LCAE, Department of Chemistry, Faculty of Science, University Mohamed I , P.O. Box 524, Oujda 60 000, Morocco.*

[3] *LAQV-REQUIMTE, Department of Chemistry, University of Aveiro, 3810-193 Aveiro, Portugal.*

[4] *Department of Electrical Engineering and Computer Science & Research Center MANSiD, "Stefan cel Mare" University, University Street, No. 13, Suceava 720229, Romania.*

* *Corresponding authors:* radi@ump.ac (S. Radi), yann.garcia@uclouvain.be (Y. Garcia) and nmoura@ua.pt (N.M.M. Moura)

Abstract

In this work, two new hybrid materials, **MP$_1$** and **MP$_2$**, were synthesized by modifying the mesoporous silica **MCM-41** with 5,10,15,20-tetrakis(pentafluorophenyl)porphyrin as well as 5,10,15,20-tetra(pyridin-4-yl)porphyrin, respectively. The successful modification was consistently confirmed through multiple characterization techniques. The adsorption performance of these hybrid systems for Cd(II), Cu(II) and Pb(II) ions was thoroughly investigated using different isotherm and kinetic models to understand the adsorption mechanism. Both materials exhibited significant affinity for Pb(II) ions, with maximum adsorption capacities of 265.70 mg/g for **MP$_1$** and 77.69 mg/g for **MP$_2$**, surpassing many previously reported systems. The adsorption process was remarkably fast, reaching 65 % of maximum uptake within 10 min and complete removal from solution within 45 min. Selectivity studies showed that these adsorbents efficiently removed 70 % of Pb(II) ions even in the presence of Cd(II) and Cu(II) ions at similar concentrations. Furthermore, both adsorbents demonstrated excellent reusability, maintaining high efficiency over five consecutive cycles with minimal capacity loss. Most importantly, their performance was validated using real river water samples from the Marchica River, achieving up

to 89 % Pb(II) removal at trace concentrations. The adsorption equilibrium and kinetic data fitted well to the Sips, Langmuir, and pseudo-second-order models ($R^2 > 0.99$), indicating a homogeneous monolayer adsorption mechanism dominated by chemisorption. Thermodynamic parameters ($\Delta G < 0$, $\Delta H > 0$) showed that the adsorption was endothermic, spontaneous and became more favorable at higher temperatures. These results highlight the strong potential of porphyrin conjugation with mesoporous silica **MCM-41** to develop efficient, selective, and cost-effective adsorbents for toxic metal ions removal in practical applications.

Keywords: MCM-41; Mesoporous silica; Porphyrin; Adsorption; Water pollution; Hazardous metal ions.

1. Introduction

Lead is among primary dangerous heavy metals, causing serious threats to both environment and humans.[1–3] Its ubiquitous use in industries including battery manufacturing,[4] mining,[5] and paint production[6] has contaminated water sources, soils and even the atmosphere.[7] Lead exposure may permanently harm the nervous system,[8] especially in children cases, resulting in cognitive deficits and developmental difficulties.[9] In adults, it has been associated to many diseases, for instance, to kidney failure, cardiovascular diseases, and reproductive toxicity.[10–12] Due to its non-biodegradable nature, lead remains in the environment for lengthy periods of time, making removal a difficult task.

Water contamination with lead, in particular, poses serious environmental and health risks, as exposure to levels exceeding the World Health Organization's (WHO) recommended limit of 10 µg/L can lead to severe toxic effects.[13] A striking example of this issue is the Marchica River in Nador - Morocco, which has been reported to contain dangerously high concentration of lead due to industrial and agricultural discharge as well as urban runoff.[14] Despite numerous cleanup efforts, eliminating or reducing the concentration of trace metals below the recommendation limits remains a major challenge, requiring advanced treatment techniques. Tackling this issue is essential to protecting both aquatic ecosystems and public health. Accordingly, there is a need for adsorbents that combine high metal ion selectivity with fast uptake, operational robustness, and validation in real environmental waters. Several techniques have been developed to extract lead from contaminated water, including chemical precipitation, ion exchange, electrocoagulation and

membrane filtration. While these methods can be effective under specific conditions, they often come with significant drawbacks.[15,16] In practice, excessive reagent use, sludge formation, high costs, fouling and scale-up challenges limit their implementation.[17] Accordingly, the need for efficient adsorbents has prompted several research groups to develop materials with high selectivity for different metal ions, fast uptake, and efficient regeneration capability.[18]

Among the various strategies, adsorption has gained significant attention due to its simplicity, cost-effectiveness, and high efficiency in removing heavy metals.[19,20] The development of hybrid materials combining inorganic supports with organic functional groups has revolutionized adsorption technology, enhancing selectivity and capacity across diverse aplications.[21–27]

In the context of metal ion adsorption, the inorganic support provides a stable, high-surface-area structure, while organic functional groups offer specific binding sites for target metal ions. The success of these materials heavily depends on the choice of the inorganic support and organic functionalities, which influence adsorption strength and speed.[28–30] However, few systems simultaneously demonstrate (i) high and selective Pb(II) uptake, (ii) rapid kinetics, (iii) multi-cycle reusability, and (iv) maintained performance in real waters containing competing ions and organic matter, features required for practical application.

Compared with conventional silica, **MCM-41** silica is a particularly attractive alternative for hybrid materials in adsorption applications, due to its high surface area, uniform mesoporous structure and large pore volume, which facilitates better diffusion and uptake of larger molecules as well as its good thermal stability.[31,32] Considering the range of organic functionalities available to decorate material surface, particular attention is being given to porphyrins. This class of tetrapyrrolic macrocycles, has shown exceptional potential in heavy metal adsorption due to their ability to form stable coordination complexes with metal ions. Their nitrogen-rich core allows strong interactions with transition metals, significantly improving adsorption performance. In particular, 5,10,15,20-tetrakis(pentafluorophenyl)porphyrin (**P_1**) is of great interest due to the strong electron-withdrawing effect of fluorine atoms. These fluorine substituents enhance the Lewis acidity of the nitrogen centers, increasing their affinity for lead(II) ions as demonstrated previously by our group after immobilizing it in conventional silica.[33] Incorporating **P_1** into an inorganic framework such as mesoporous **MCM-41** can provide a highly effective adsorbent with well-structured porosity, high surface area, and excellent stability.[34–36] In this design, the

mesoporous channels of MCM-41 are expected to maximize the accessibility and density of porphyrinic N-donor sites, favoring inner-sphere Pb–N coordination that should enable fast and selective capture.

Given that 5,10,15,20-tetrakis(pentafluorophenyl)porphyrin derivatives with additional pyridyl ligands, showed efficient adsorbents features towards a wide range of metal ions,[25,37] and 5,10,15,20-tetra(pyridin-4-yl)porphyrin is easily accessible,[38] **MCM-41** silica-based adsorbents incorporating this macrocycle, could offer a promising alternative. By immobilizing two structurally distinct porphyrins on the same MCM-41 scaffold, this work also analyzes how ligand electronic, charge and coordination features influence performance, providing mechanistic insight beyond prior porphyrin–silica adsorbents.

In this work, we report the synthesis and characterization of two modified **MCM-41** materials, **MP$_1$** and **MP$_2$**, incorporating 5,10,15,20-tetrakis(pentafluorophenyl)porphyrin (**P$_1$**) as well as 5,10,15,20-tetra(pyridin-4-yl)porphyrin (**P$_2$**) respectively, as organic ligands for Pb(II), Cd(II), and Cu(II) ions adsorption application. The hybrids were comprehensively characterized to confirm successful porphyrin immobilization within MCM-41. The novelty and advantages are: simple and scalable synthesis; selective and rapid Pb(II) adsorption; robust five-cycle reusability; and high removal efficiency in real river water, collectively addressing key practical gaps and bridging adsorption for efficient and cost effective scalable solution.

To evaluate the adsorption performance of **MP$_1$** and **MP$_2$**, we conducted a series of batch experiments investigating various parameters, including initial metal concentration, contact time, pH and temperature. Adsorption kinetics and isotherm models were applied to understand the adsorption mechanism and determine the materials' efficiency. The selectivity studies were performed to assess the competitive adsorption of Pb(II) ions in the presence of Cd(II) and Cu(II) ions, demonstrating the strong affinity of the prepared materials for Pb(II) ions. The reusability of **MP$_1$** and **MP$_2$** was also tested over multiple cycles (5 cycles), revealing minimal efficiency loss, which is a key factor for affordability and sustainability.[39] Furthermore, real-world applicability was investigated using water samples from the Marchica River. The prepared materials **MP$_1$** and **MP$_2$** demonstrated exceptional performance in lead(II) removal, even at trace concentrations, further proving their potential for real environmental remediation. Taken together, these elements clarify the uniqueness and practical relevance of the present study within the broader field of heavy-metal adsorption.

2. Results and discussion

2.1. Synthesis of the adsorbents

The synthesis of **MP$_1$** and **MP$_2$** involved the two main steps, as outlined in Scheme 1. The first step consisted on the surface functionalization of **MCM-41** with the organosilane groups (3-aminopropyl)trimethoxysilane (APTMS) and (3-chloropropyl)trimethoxysilane (CPTMS) to afford the functionalized silica **MCM-41-NH$_2$** and **MCM-41-Cl**, respectively.[40] The second step involved the direct reaction of **MCM-41-NH$_2$** with 5,10,15,20-tetrakis(pentafluorophenyl)porphyrin (**P$_1$**) (Via A) and **MCM-41-Cl** with 5,10,15,20-tetra(pyridin-4-yl)porphyrin (**P$_2$**) (Via B), affording the required materials, **MP$_1$** and **MP$_2$**, respectively. Both porphyrin ligands were prepared by condensation of pyrrole with the appropriate aldehyde according to well-established procedures reported in the literature.[41–43] The immobilization step relied on the easy substitution of *p*-fluorine atoms in **P$_1$**'s pentafluorophenyl units by amines and the quaternization of pyridyl units in **P$_2$** by alkylating agents.[38,44]

To determine the exact amount of porphyrin required for immobilization onto the surface of **MCM-41** before reaching saturation, a preliminary assay was performed. Small portions of **P$_1$**, and **P$_2$** (30 mg each) were progressively added to the appropriate silica (2 g), and the presence of residual ligands was checked by thin-layer chromatography (TLC) after 4 h of reflux under N_2 atmosphere. This method showed that the functionalized **MCM-41** silica reached saturation after the addition of 150 mg of porphyrins.

Considering the results from the previous assay, the reactions of **MCM-41-NH$_2$** with **P$_1$** in toluene and **MCM-41-Cl** with **P$_2$** in *o*-dichlorobenzene were carried out at reflux under a N_2 atmosphere for two days, using 2 g of silica and 150 mg of each ligand (Scheme 1). The adsorbents were separated from the solution by centrifugation and washed with the reaction solvent and methanol until no porphyrin was detected in the washing solvent.

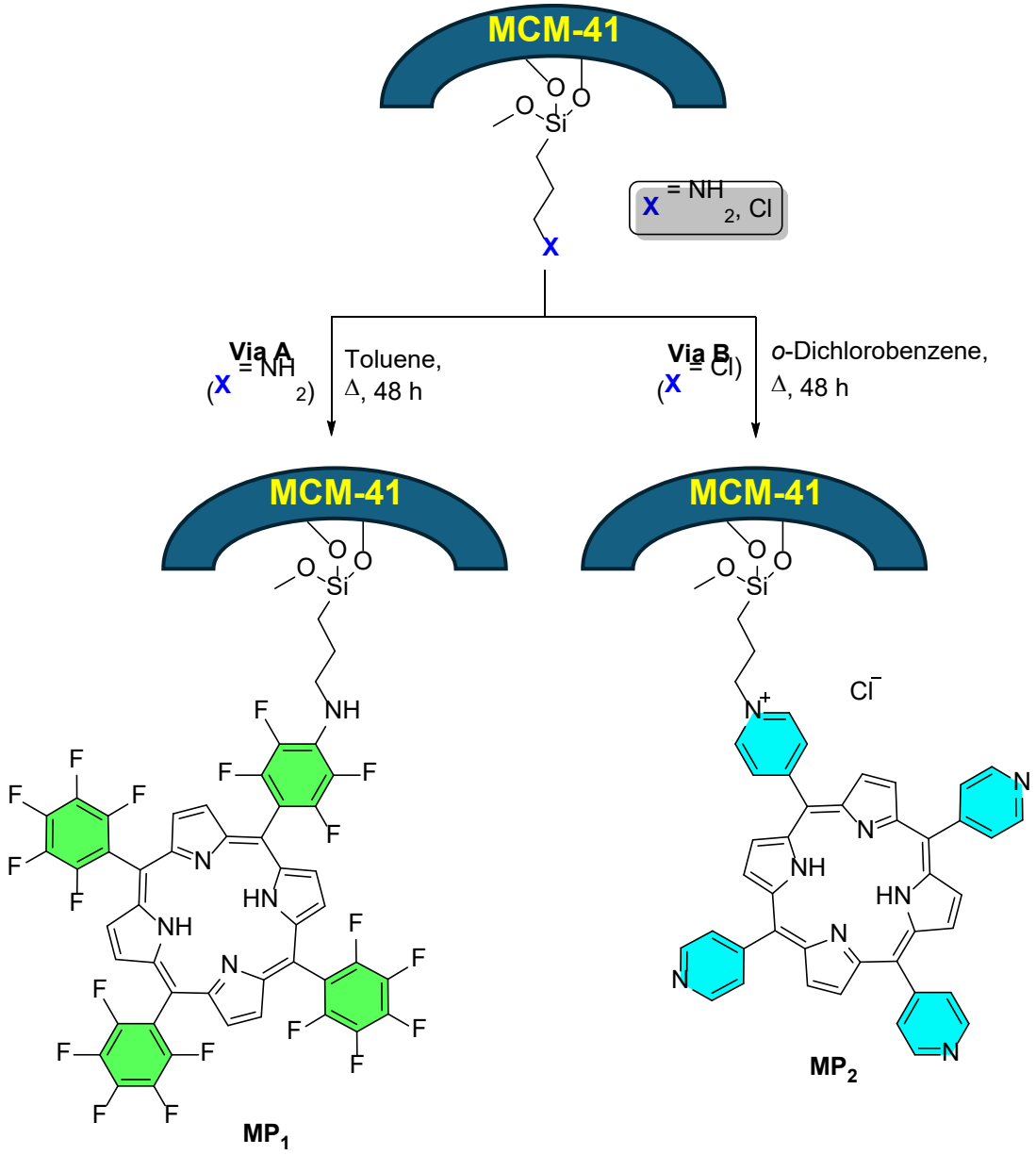

Scheme 1. Synthetic approaches used in the preparation of **MP1** (Via A) and **MP2** (Via B) from the functionalized precursors **MCM-41-NH2** and **MCM-41-Cl**, respectively.

2.2. Characterization of materials MP1 and MP2

2.2.1. FT-IR spectra analysis

Figure 1 presents the ATR-FTIR spectra of the materials **MP1** and **MP2** in comparison to their respective functionalized **MCM-41**. In all the spectra, characteristic bands of the silica can be observed, including an intense peak near 3440 cm^{-1} which is associated with the O-H stretching

vibrations of silanol groups. Other significant peaks include one at around 1635 cm^{-1}, corresponding to the Si-OH stretching vibration, and another at 1090 cm^{-1}, linked to the Si-O-Si stretching vibration. Additionally, the band at approximately 807 cm^{-1} is attributed to Si-O vibrations.[45] After the modification with porphyrin molecules, new peaks emerged at 1460, 1500 cm^{-1} as well as a notable one around 750 cm^{-1} indicating the appearance of stretching vibrations of C-C bonds in porphyrin ligands.[46] More specifically, the peaks in the range of 1390-1574 cm^{-1} (highlighted in green in **Figure 1**) are mainly attributed to the C=N and C=C vibration of the aromatic rings.

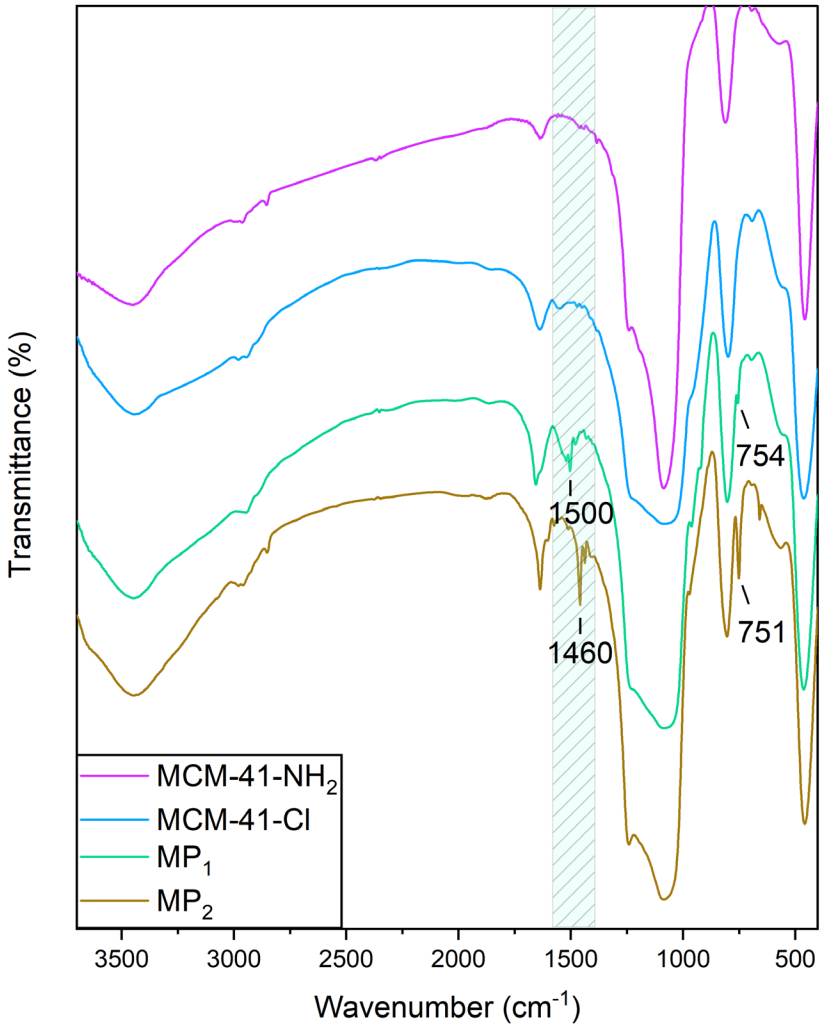

Figure 1. ATR-FTIR spectra of **MP_1** and **MP_2**, and of respective functionalized **MCM-41-NH_2** and **MCM-41-Cl**.

2.2.2. UV-Visible analysis

Figure 2 shows the solid-state UV-Vis spectra of **MP1** and **MP2**. We observe the characteristic absorption features of *meso*-tetraarylporphyrins.[25] These include a prominent Soret band at $\lambda = 412$ nm for **MP1** and $\lambda = 433$ nm for **MP2**, followed by weaker four Q bands extending from 510 to 657 nm. This spectral profile is consistent with the expected electronic transitions of porphyrin-based systems. Thus, providing additional proof of the successful porphyrin immobilization onto the **MCM-41** surface.

To check the absence of free porphyrin species in the final materials and during use, the freshly prepared hybrids were exhaustively washed; the combined wash filtrates were then analyzed by liquid-phase UV–Vis. No Soret or Q-band signatures characteristic of free porphyrins were detected. These results confirm covalent immobilization, the absence of porphyrin leaching, and environmentally benign behavior of the hybrid adsorbents during water treatment.

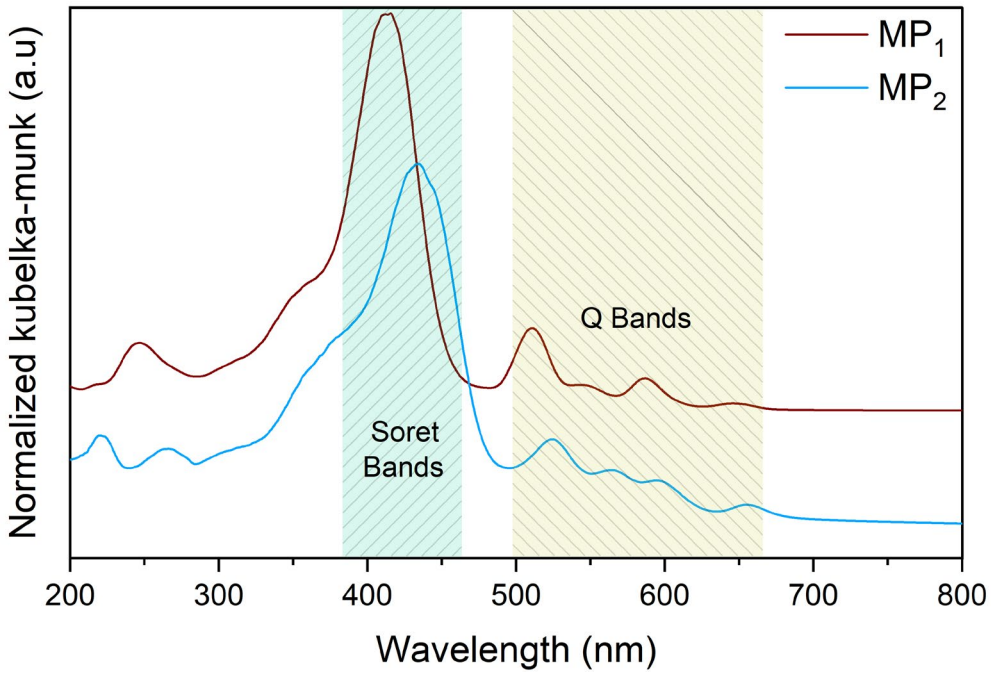

Figure 2. Solid state UV-Vis spectra of **MP1** and **MP2**.

2.2.3. Elemental analysis

Table 1 summarizes the elemental analysis results of the adsorbents **MP1** and **MP2** and of the precursors: **MCM-41**, **MCM-41-NH2** and **MCM-41-Cl**. The carbon and nitrogen contents of

MCM-41 before functionalization are negligible. Upon functionalization with CPTMS, the resulting **MCM-41-Cl**, exhibited a significant increase in the carbon content (7.65 %), followed by a moderate increase in the hydrogen content (1.76 %), while the nitrogen level remained negligible. Functionalization with APTMS to obtain **MCM-41-NH_2**, led to significant increases in both carbon (5.94 %) and nitrogen (2.00 %) contents, as expected due to the presence of amino groups in the organosilane reagent. Following the incorporation of **P_1** and **P_2**, the resulting **MP_1** and **MP_2** materials displayed additional increases in both carbon and nitrogen content, which aligns with the inherent composition of porphyrins, known for their high carbon and nitrogen content.

Table 1. Elemental analysis results of **MCM-41**, functionalized supports, and adsorbents **MP_1** and **MP_2**

Sample	C%	H%	N%
MCM-41	0.05	0.65	0.10
MCM-41-NH_2	5.94	1.60	2.00
MP_1	7.35	2.09	2.29
MCM-41-Cl	6.12	1.25	0.01
MP_2	9.56	1.32	1.24

2.2.4. Solid state ^{13}C NMR spectroscopy

Solid-state ^{13}C NMR analysis highlights the appearance of new peaks after the mesoporous silica is functionalized and modified. The spectra for both precursors **MCM-41-NH_2** and **MCM-41-Cl** are very similar, as shown in **Figure S1** (ESI). These functionalized materials display signals in the aliphatic region at around δ 8, 25, and 45 ppm, corresponding to the carbon atoms in the Si-CH_2-CH_2-CH_2-NH_2 (or -Cl) chains. When ligands **P_1** and **P_2** were introduced, additional signals emerge, ranging from ca. δ 105 to 154 ppm, which are due to the resonance of the aromatic carbons from the porphyrins core.[33] On the other hand, the ^{13}C NMR signal near δ 50 ppm is primarily attributed to non-substituted methoxy groups (-OCH_3).

2.2.5. Thermogravimetric analysis

The thermal stability of the adsorbents **MP_1**, **MP_2** as well as their respective precursors was studied utilizing thermogravimetric analysis. **Figures S2** to **S6** (ESI, online resource) highlight the percentage of weight loss from 25 °C to 800 °C. All materials experienced relative weight loss

between 25 to 110 °C due to the adsorbed water molecules on the surface of the mesoporous silica, as it is frequently reported in the literature.[47] Moreover, in the temperature range between 110 °C and 800 °C (highlighted in yellow), a weight loss of 3.74 % was observed for **MCM-41** (**Figure S2**), mainly due to the degradation of the condensed free silanol groups present on the surface. After functionalization, both **MCM-41-NH$_2$** and **MCM-41-Cl** showed a much higher degradation, with weight losses of 7.47 % (**Figure S3**) and 9.28 % (**Figure S4**) respectively.[48,49] This is assigned to the decomposition of the organic silane agents immobilized on the surface (APTMS and CPTMS).

Following the addition of porphyrins **P$_1$** (**Figure S5**) and **P$_2$** (**Figure S6**), mass losses of 9.39 % for **MP$_1$** (compared to 7.47 % for **MCM-41-NH$_2$**) and of 10.82 % for **MP$_2$** (compared to 9.28 % for **MCM-41-Cl**) confirmed the successful grafting of these porphyrins onto the mesoporous silica.

2.2.6. BET/BJH analysis

Figure 3 displays the N_2 adsorption–desorption isotherm of the new adsorbents **MP$_1$** and **MP$_2$** as well as the precursors **MCM-41**, **MCM-41-NH$_2$** and **MCM-41-Cl.** The curves exhibit a type IV profile, characteristic of mesoporous solids, as indicated in the literature.[50] The isotherms, which showed consistent pore channels, were extremely similar, indicating complementary textural features and framework-confined mesoporous systems.

Additionally, on Table 2 are summarized the physical surface parameters of materials M**P$_1$** and **MP$_2$** as well as of their precursors, including the surface area (S_{BET}) and pore volume (V_{pore}) values obtained from Brunauer-Emmett-Teller (BET) surface area and Barrett-Joyner-Halenda (BJH) pore size analyses. The functionalization of **MCM-41** with APTMS and CPTMS was responsible for a reduction in its surface area from 781.86 m^2/g to 694.55 m^2/g and 707.14 m^2/g for **MCM-41-NH$_2$** and **MCM-41-Cl** respectively. It can also be observed that the pore volume size also decreased accordingly by approximately 29 %. Moreover, the attachment of porphyrin molecules onto the functionalized supports drastically lowered the surface area to 205.42 m^2/g and 307.87 m^2/g, accompanied by an additional pore size volume decrease of 39 % and 48 % respectively. These reductions are related to the introduction of porphyrin ligands onto the mesoporous silica surface, which hinders the adsorption of N_2 molecules. In summary, the overall

findings consistently demonstrate that surface modification leads to a reduction in both surface area and pore volume.

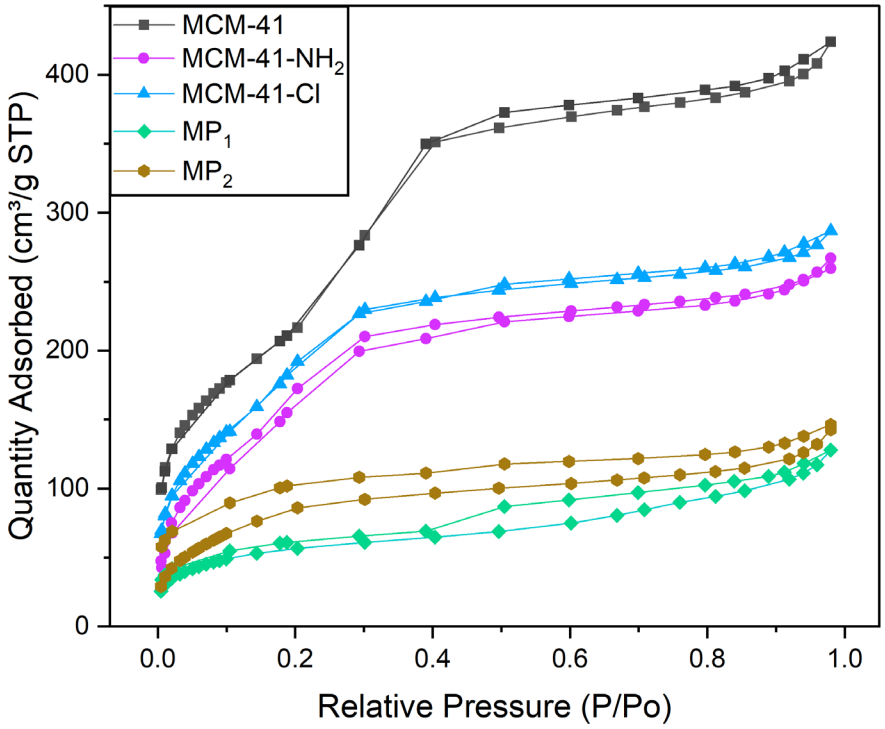

Figure 3. N_2 Adsorption-Desorption isotherm of **MP_1**, **MP_2** and their respective precursors.

Table 2. Physical surface parameters of materials **MP_1** and **MP_2** and their respective precursors.

Materials	S_{BET} (m^2/g)	V_{pore} (cm^3/g)
MCM-41	781.8610	0.79581
MCM-41-NH_2	694.5477	0.56421
MP_1	205.4241	0.21945
MCM-41-Cl	707.1388	0.57581
MP_2	307.8699	0.27739

2.2.7. Scanning electron microscope

Scanning electron microscope (SEM) was used to study the morphological changes in **MCM-41**, **MCM-41-NH_2**, and **MCM-41-Cl** as well as in the final hybrids **MP_1** and **MP_2** after the corresponding modifications; the images obtained are displayed in **Figure 4**. The texture of **MCM-41,** before any functionalization, seems spongy and hazy. After the functionalization with the

organo-silane groups, the surface becomes more irregular and loses its hazy appearance. Furthermore, both materials produced upon porphyrin attachment exhibit agglomerated spherical shapes, which is a typical feature indicative of organic alteration of this material class.[51]

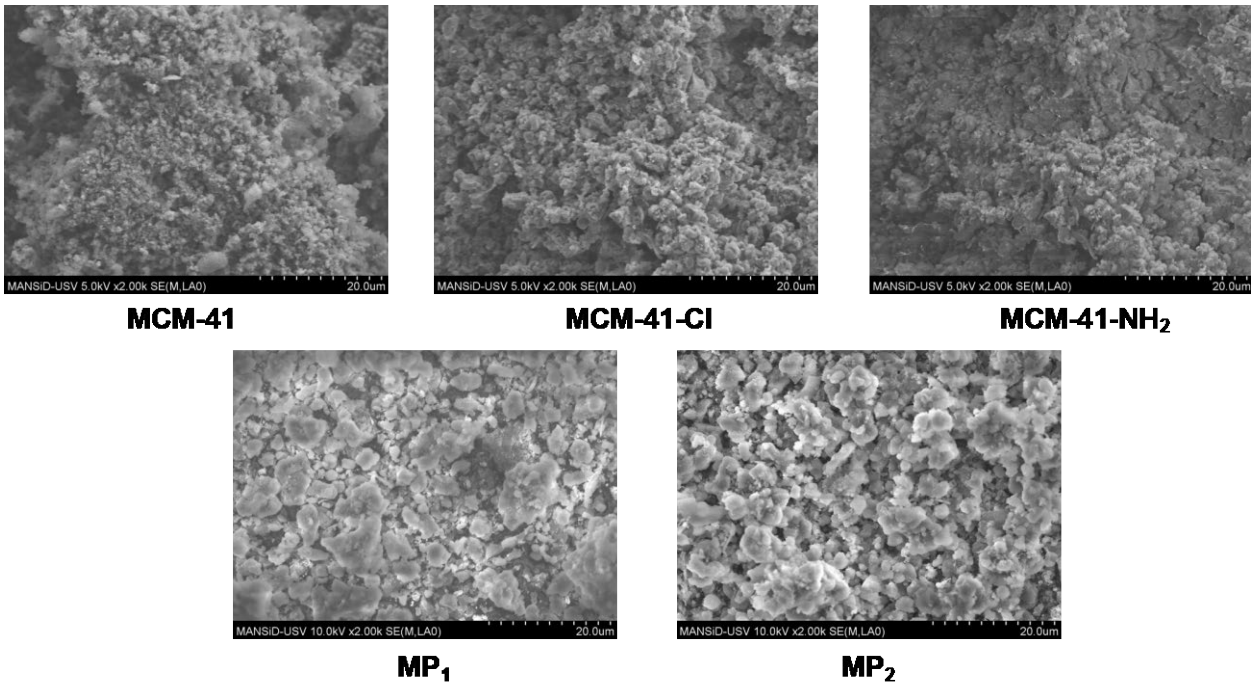

Figure 4. Scanning electron microscopy (SEM) of precursors (top) and adsorbents (bottom).

2.3. Evaluation of the hazardous metal ions adsorption efficiency of the new MP_1 and MP_2 conjugates

2.3.1. Initial metal concentration effect on the adsorption and isotherm models

The adsorption performance of the new hybrids **MP_1** and **MP_2** for Cd(II), Cu(II), and Pb(II) ions, was evaluated through several assays, including the effect of the initial metal ion concentration on their adsorption capacity (Figure 5).

To better understand the adsorption mechanism in each process, the experimental adsorption capacities of each adsorbent were fitted to four nonlinear adsorption isotherm models: Langmuir, Freundlich, Temkin, and Sips (see equations and references in Table 3). The results are summarized in Table 4.

The adsorption capacities of **MP_1** and **MP_2** were determined in aqueous solution using 10 mg of each material in 10 mL of solution, with metal ion concentrations ranging from 10 to 500

mg/L. The experiments were conducted at pH 6 and 298 K, with a 2 h contact time. As shown in Figure 5, both materials exhibited positive adsorptions for all tested metal ions, with **MP$_1$** displaying a particularly high Pb(II) ion extraction capacity. Furthermore, this experiment helped determining the optimal metal ion concentration for both materials, as summarized in Table 10 (see experimental section).

Notably, **MP$_1$** achieved an impressive adsorption value of 265.7 mg/g for Pb(II) ion, which, to our knowledge, is among the highest, if not the highest, reported in the literature for silica-based adsorbents. This excellent performance is primarily attributed to the grafted 5,10,15,20-tetrakis(pentafluorophenyl)porphyrin (**P$_1$**), which provides abundant nitrogen donor sites for metal ion binding. Additionally, the strong electron-withdrawing effect of the fluorine significantly enhances nitrogen's coordination.as previously reported.[33] However, the choice of **MCM-41,** as the immobilization support played also a crucial role in this enhancement. Compared to our previous study using the same ligand on commercial silica gel (60 Å), which achieved an adsorption value of 187.4 mg/g,[33] this represents an improvement of approximately 42 %, highlighting the advantages of **MCM-41** as a superior support for metal ion adsorption.

MP$_1$ also demonstrated excellent adsorption performance for Cu(II) and Cd(II) ions, with adsorption capacities of 172.9 mg/g and 99.7 mg/g, respectively, values that are rarely reported in heavy metal removal studies. Compared to our previous study, this represents a significant improvement of 38 % for Cu(II) and 19 % for Cd(II), where adsorption values were 125.2 mg/g and 82.4 mg/g respectively.[33] It is worth noting that the mesoporous silica framework of **MCM-41** provides a large surface area, facilitating high grafting yields. In fact, the amount of porphyrin grafted in the functionalized **MCM-41** (150 mg in 2 g of functionalized **MCM-41-NH$_2$**) was around double the amount of what we have reported in our previous study (150 mg in 4 g of amino-functionalized silica).

In contrast, **MP$_2$** exhibited significantly lower adsorption performance, with a Pb(II) ion extraction capacity of 77.7 mg/g. The extraction capacities for Cu(II) and Cd(II) were 43.5 mg/g and 30.1 mg/g, respectively. This lower efficiency when compared with the results obtained with **MP$_1$** and also with **P$_1$** derivatives bearing additional pyridyl units is primarily due to the positive charge generated on the pyridyl ring upon grafting, which increases electrostatic repulsion between the adsorbent and the positively charged metal cations. Additionally,-the possible attachment of multiple pyridyl units to the support likely restricts their ability to act as additional ligands. Despite

this, **MP₂** still demonstrated good adsorption capacities compared to similar materials reported in the literature.[52]

Table 4 shows that the Sips and Langmuir models provided the best fit for the adsorption process, with correlation coefficient (R^2) values exceeding 0.990. The adsorption capacity predicted by these models closely matched the experimental value (Q_{exp}), suggesting a predominantly homogeneous mechanism, involving monolayer adsorption. This is further supported by the observed saturation point at higher concentrations, aligning with previous studies.[53,54]

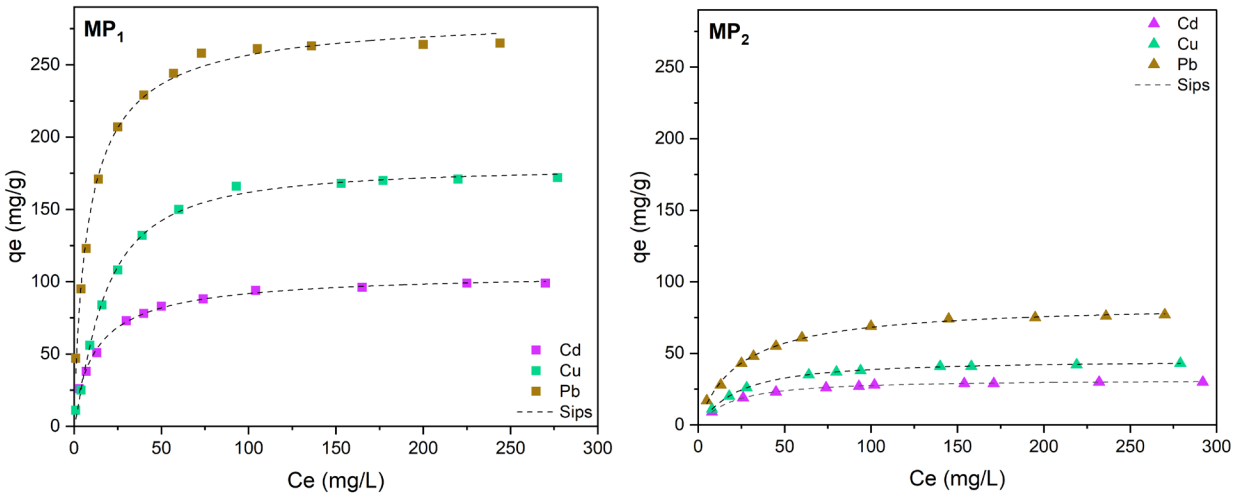

Figure 5. Effect of the initial concentration of each metal ion Cd(II), Cu(II) and Pb(II) on the adsorption capacity of **MP₁** (left) and **MP₂** (right). Adsorption conditions: 10 mg of adsorbents in 10 mL of an aqueous solution containing each metal ion at a concentration ranging from 10 to 500 mg/L, at 298 K, pH 6.0 and a contact time of 2 h. Experimental adsorption data fitted using Sips isotherm model.

Table 3. Nonlinear equations of adsorption isotherm.

Isotherm Model	Equations	References
Langmuir	$q_e = \frac{K_L Q_L C_e}{1 + K_L C_e}$	55
Freundlich	$q_e = K_F {C_e}^{1/n_F}$	56
Temkin	$q_e = B_T \ln A_T C_e$	57
Sips	$q_e = \frac{K_S Q_S {C_e}^{1/n_S}}{1 + K_S {C_e}^{1/n_S}}$	58

C_e: Equilibrium concentration of metal in solution (mg/L); q_e: Amount of metal adsorbed per unit mass of adsorbent (mg/g); Q_L: Maximum adsorption capacity in the Langmuir model (mg/g); K_L: Langmuir constant related to adsorption energy (L/mg); K_F: Adsorption capacity in the Freundlich model (L/g); n_F: Adsorption intensity in the Freundlich model; B_T: Temkin constant related to adsorption heat (BT = RT/bT); **bT**: Temkin isotherm constant; A_T: Temkin equilibrium binding constant (L/g), representing maximum binding energy; Q_S: Maximum adsorption capacity in the Sips model (mg/g); K_S: Sips equilibrium constant (L/mg); $1/n_S$: Sips model exponent.

Figure 6. Effect of the initial concentration of each metal ion Cd(II), Cu(II) and Pb(II) on the adsorption capacity of **MP1** (left) and **MP2** (right). Adsorption conditions: 10 mg of adsorbents in 10 mL of an aqueous solution containing each metal ion at a concentration ranging from 10 to 500 mg/L, at 298 K, pH 6.0 and a contact time of 2 h. Experimental adsorption data fitted using Sips isotherm model.

Table 4. Isotherm adsorption models parameters and experimental adsorption capacities.

Isotherm Model	Adsorbent	MP_1			MP_2		
	Metal	Cd(II)	Cu(II)	Pb(II)	Cd(II)	Cu(II)	Pb(II)
Langmuir	Q_L	103.16	185.69	275.06	32.48	47.27	80.20
	Q_{exp}	99.7	172.9	265.7	30.1	43.5	77.7
	K_L	0.083	0.048	0.120	0.052	0.042	0.041
	R^2	0.993	0.994	0.992	0.996	0.997	0.995
Freundlich	n_F	4.017	2.856	3.628	4.264	3.586	3.301
	K_F	28.4	30.95	76.83	8.71	9.85	15.93
	R^2	0.910	0.912	0.933	0.864	0.894	0.920
Temkin	B_T	18.21	35.61	48.62	5.85	9.26	16.64
	A_T	1.460	0.817	2.284	0.891	0.530	0.543
	R^2	0.974	0.960	0.982	0.942	0.964	0.978
Sips	n_S	1.170	0.825	1.220	0.893	0.872	1.015
	Q_S	103.76	178.65	272.17	31.54	45.29	79.78
	Q_{exp}	99.7	172.9	265.7	30.1	43.5	77.7
	K_S	0.108	0.030	0.152	0.039	0.029	0.043
	R^2	0.997	0.998	0.997	0.999	0.999	0.995

2.3.2. Effect of contact time on the adsorption and kinetic models

The adsorption rate of heavy metal ions by an adsorbent is crucial for a potential practical application. Therefore, the adsorption rates of **MP₁** and **MP₂** were determined at the optimal concentration for each metal ion (see values in Table 10, experimental section) by conducting adsorption studies with 10 mg of each adsorbent at pH 6 and 298 K, with metal ion removal monitored at intervals from 5 to 60 min. The results shown in Figure 6 were analyzed using four nonlinear kinetic models: pseudo-first-order, pseudo-second-order, Elovich, and intraparticle diffusion (see Table 5 for equations).

The evolution of the adsorption rate as a function of stirring time, presented in Figure 6, shows that both hybrid materials exhibit similar behavior with respect to contact time variation, demonstrating a rapid adsorption rate within the first few minutes. After 10 min, **MP₁** and **MP₂** had already extracted more than 65 % of the maximum concentration of all metals, followed by a gradual increase until reaching the maximum at 45 min.

Table 6 highlights the kinetic parameters of the models used, as well as their correlation coefficients. Based on the results obtained, the pseudo-second-order model appears to best fit the data, as R^2 is consistently higher than 0.990. This suggests that adsorption is controlled by chemisorption, where metal ions adhere to the adsorbent surface by forming coordination bonds and tend to occupy sites that maximize their coordination with the surface.[59] Mechanistically, Pb(II) forms inner-sphere complexes with the N-donor sites of the immobilized porphyrins (porphyrinic nitrogens and proximal amino/pyridyl functions), yielding multi-dentate Pb–N coordination that is stabilized by confinement within the MCM-41 mesopores. Consistent with HSAB considerations, the borderline-soft Pb(II) preferentially binds these nitrogen donors rather than surface silanols, which rationalizes the potential high selectivity, rapid uptake, and the maintenance of capacity over regeneration cycles.

Table 5. Nonlinear equations of kinetic models.

Isotherm Model	Equations	References
Pseudo 1st order	$q_t = Q_1(1 - e^{-K_1 t})$	[60]
Pseudo 2nd order	$q_t = \frac{K_2 {Q_2}^2 t}{1 + K_2 Q_2 t}$	[61]

Elovich	$q_t = \frac{1}{\beta}\ln(1+\alpha\beta t)$	62
Intraparticle diffusion	$q_t = K_{id}t^{1/2} + C$	63

Q₁ and ***Q₂***: pseudo-first-order and pseudo-second-order equilibrium concentration respectively (mg/g); ***qₜ***: amount adsorbed (mg/g); ***t***: time (min). ***K₁*** and ***K₂***: rate constant of pseudo-first-order and pseudo-second-order, respectively (min^{-1}); ***α***: initial adsorption rate constant (g mg^{-1} min^{-1}), describing the rate of adsorption at $t = 0$; ***β***: desorption constant(g/mg); ***K_id***: diffusion rate constant (mg $min^{1/2}$ g^{-1}); ***C***: constant (mg/g)

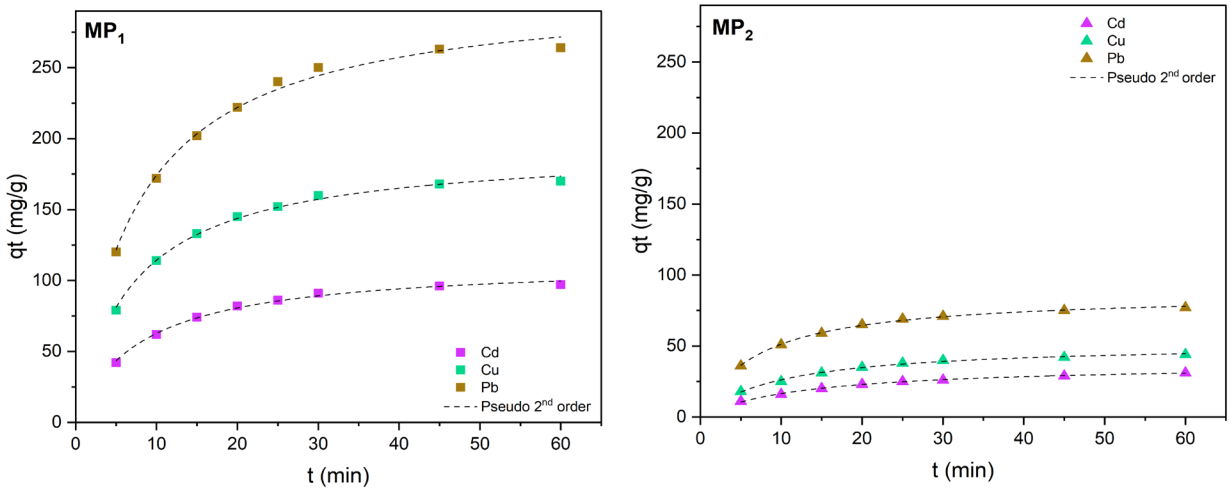

Figure 6. Effect of contact time on the adsorption rate of **MP₁** (left) and **MP₂** (right). Adsorption conditions: 10 mg of adsorbents in 10 mL of an aqueous solution containing the optimal concentration of each metal ion (see Table 10) at pH 6.0 and 298 K for periods varying between 5 min and 60 min. Experimental adsorption data fitted using the pseudo-second order model.

Table 6. Kinetic parameters of pseudo-first order, pseudo-second order, Elovich models for adsorption processes and intraparticle diffusion models.

Kinetic models	**Adsorbent**	**MP₁**			**MP₂**		
	Metal	**Cd(II)**	**Cu(II)**	**Pb(II)**	**Cd(II)**	**Cu(II)**	**Pb(II)**
Pseudo 1st order	Q_1	95.53	165.95	258.90	30.24	43.04	74.48
	K_1	0.103	0.114	0.107	0.074	0.089	0.114
	R^2	0.909	0.982	0.980	0.983	0.983	0.978
Pseudo 2nd order	Q_2	102.83	183.58	277.75	31.41	46.75	80.87
	K_2	0.001	0.001	0.001	0.002	0.002	0.002

	R^2	0.993	0.996	0.993	0.996	0.996	0.994
Elovich	α	30.77	30.16	93.50	4.66	9.92	31.48
	β	0.042	0.026	0.016	0.108	0.086	0.058
	R^2	0.945	0.944	0.944	0.988	0.965	0.954
Intraparticle diffusion	C	32.27	64.4	92.90	5.29	11.50	28.72
	K_{id}	9.614	15.698	25.335	3.585	4.679	7.065
	R^2	0.852	0.847	0.856	0.943	0.896	0.863

2.3.3. Thermodynamic studies

Analyzing thermodynamic parameters such as enthalpy (*ΔH*), entropy (*ΔS*), and Gibbs free energy (*ΔG*) provides valuable insights into the adsorbent's behavior and the effect of temperature on adsorption. A negative *ΔH* signifies an exothermic process, while a positive *ΔH* indicates an endothermic one, meaning adsorption is enhanced at higher temperatures. Similarly, a negative *ΔS* implies a decrease in randomness at the solid-liquid interface, whereas a positive *ΔS* suggests increased disorder. As for *ΔG*, a negative value confirms that the adsorption process is spontaneous and becomes more favorable at higher temperatures, while a positive *ΔG* suggests non-spontaneous adsorption.

To determine these thermodynamic parameters, adsorption experiments were conducted at 298 K, 308 K, and 318 K for both hybrid materials, using the optimal metal ion concentration, at pH 6.0. The values were calculated using the equations outlined in the method proposed by Zhou:[64]

$$K = K_d \; x \; M_{adsorbate} \; x \; \gamma$$

$$lnK = -\frac{\Delta H}{RT} + \frac{\Delta S}{R}$$

$$\Delta G = \Delta H - T\Delta S$$

where K_d (L/g) is the experimental distribution constant, K is the equilibrium constant, γ is the coefficient of activity, and R (8.314 J mol^{-1} K^{-1}) is the ideal gas constant.

The parameters *ΔH*, *ΔS*, and *ΔG* are summarized in Table 7 and were determined from the plot of *LnK* vs *1/T* represented in Figure 7. The positive value of *ΔH* indicates an endothermic sorption, which explains the rise in adsorption concentrations with higher temperatures for transition metals. Moreover, an increase in the randomness at the interface metal/material is proved

by the positive value of *ΔS*. More importantly, the negative value of *ΔG* stipulate that the adsorption process was spontaneous and attainable even at ambient temperature. Besides, the decreases of this parameter as the temperature rises, indicate that the adsorption of ions was more favorable at higher temperature and the active sites on the surface of adsorbents were easily accessible.[65]

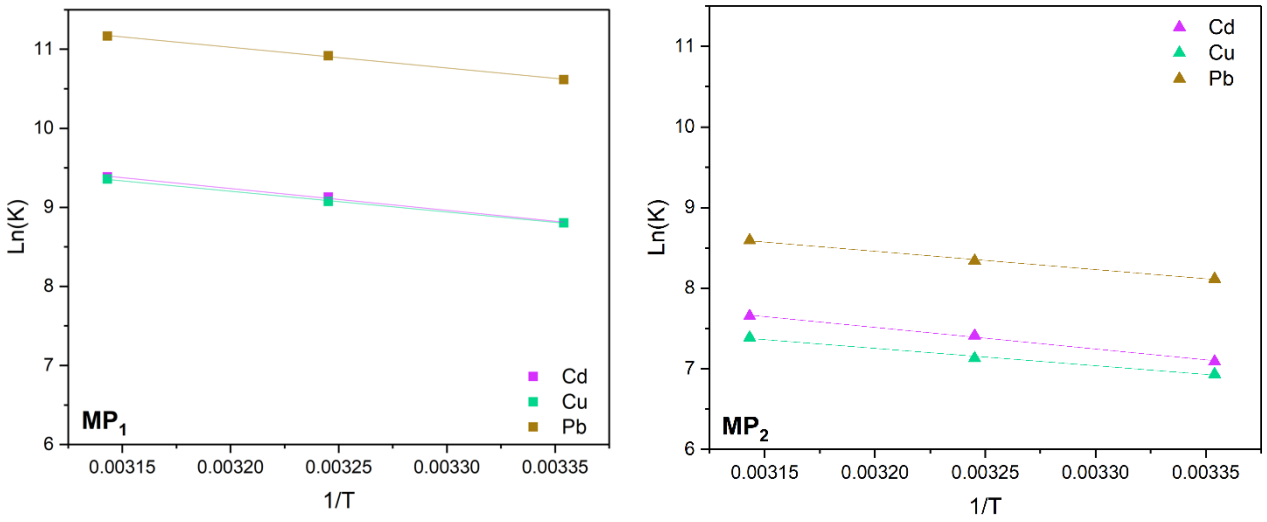

Figure 7. Effect of temperature on metal ions sorption by **MP₁** (left) and **MP₂** (right). Adsorption conditions: 10 mg of adsorbents in 10 mL of an aqueous solution containing the metal ion at its optimal concentration, at pH 6.0, for 45 min, and at temperatures of 298, 308 and 318 K.

Table 7. Thermodynamic parameters of **MP₁** and **MP₂**.

Adsorbents	Metals	ΔH° (kJ.mol^{-1})	ΔS° (kJ.K^{-1}.mol^{-1})	ΔG° (kJ.mol^{-1})		
				298 K	308 K	318 K
MP₁	**Cd(II)**	22.9178	0.1501	-21.84	-23.35	-24.85
	Cu(II)	21.8134	0.1463	-21.81	-23.27	-24.74
	Pb(II)	21.7817	0.1614	-26.33	-27.94	-29.55
MP₂	**Cd(II)**	22.2786	0.1338	-17.60	-18.94	-20.27
	Cu(II)	17.9173	0.1176	-17.15	-18.33	-19.51
	Pb(II)	18.8836	0.1307	-20.10	-21.40	-22.71

2.3.4. Effect of pH

The acidity of a solution has a critical role in adsorption by influencing surface charge and consequently the competition between protons and metal cations for binding sites.[66,67] Figure 8 displays the influence of pH (3.0 to 7.0) on the adsorption capacity of **MP₁** and **MP₂**. These assays

were performed at a shaking time of 45 min, a temperature of 298 K and at the optimal concentration of each metal ion (Table 10).

Both hybrids exhibit a similar pH-dependent trend, with a noticeable decline in adsorption performance at pH values below 4, where adsorption capacity drops to less than 47 % of its maximum. This effect can be attributed to the pronation of surface groups, reducing the number of available adsorption sites.[68] Since Cd(II) and Pb(II) have relatively large ionic radii (0.97 Å and 1.20 Å, respectively), their lower charge densities, making them highly susceptible to protonation effects. Cu(II) ions, on the other hand, behave differently due to the structure of its hydrated form. The $[Cu(H_2O)_6]^{2+}$ complex undergoes a tetragonal distortion caused by the Jahn–Teller effect, which compresses the octahedral structure along the x- and y- axes.[69] This results in four shorter bonds and two longer ones, allowing bindings mainly along the x- and y- directions while limiting interaction along the z- axis. When surface groups become more protonated, this effect is further pronounced, restricting Cu(II) adsorption even more. Overall, due to these factors, the adsorption of Cu(II), Cd(II), and Pb(II) ions is significantly diminished at lower pH, primarily through a cation exchange mechanism.

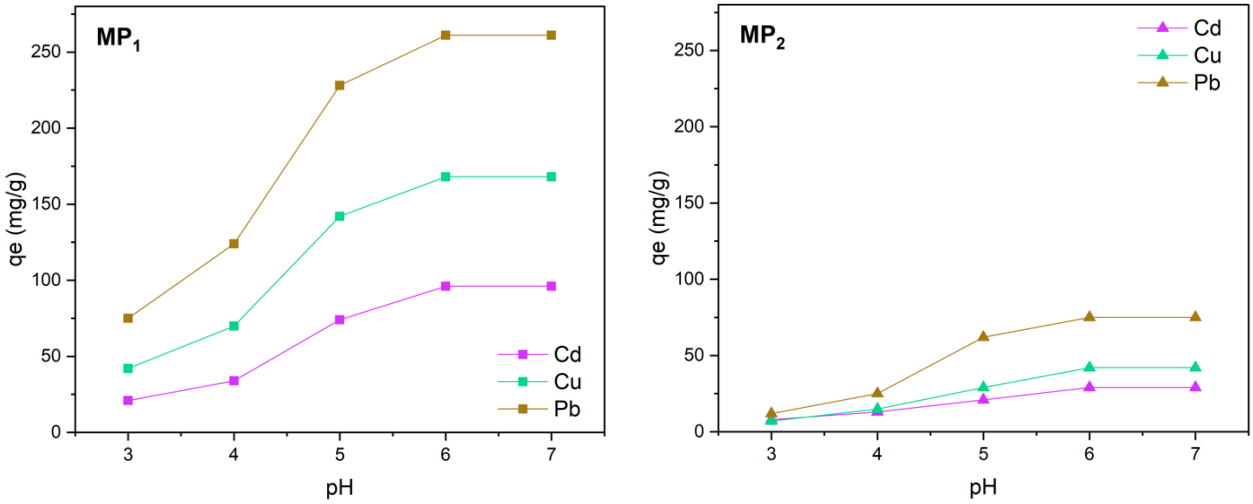

Figure 8. pH impact on the adsorption capacity of **MP1** (left) and **MP2** (right). Adsorption conditions: 10 mg of adsorbents in 10 mL of an aqueous solution containing each metal ion at its optimal metal concentration, at pH ranging from 3.0 to 7.0 for 45 min and at 298 K.

2.3.5. Selectivity performance of **MP1** and **MP2** for Pb(II)

Various materials have shown good heavy metal extraction capabilities, but their limited selectivity reduces their practicality for targeted purification.[70] Considering this, another important

aspect to assess is whether the higher selectivity of **MP1** and **MP2** for Pb(II) is affected by the presence of other metal ions. To ensure a fair comparison, adsorption assays were performed with all metal ions at the highest optimal concentration found for Pb(II): 370 mg/L for **MP1** and 210 mg/L for **MP2.** The results shown in Figure 9, indicate that both materials maintain a significant selectivity toward Pb(II) ion. In both cases the extraction of Pb(II) by **MP1** and **MP2** remains above 70 % even in the presence of the other transition metal ions. This suggests that incorporating these ligands into **MCM-41**, did not compromise their highly efficiency in extracting Pb(II) ion from aqueous solutions, regardless the presence of competing metal ions, as previously observed for **P1** attached to commercial silica gel (60 Å).[33]

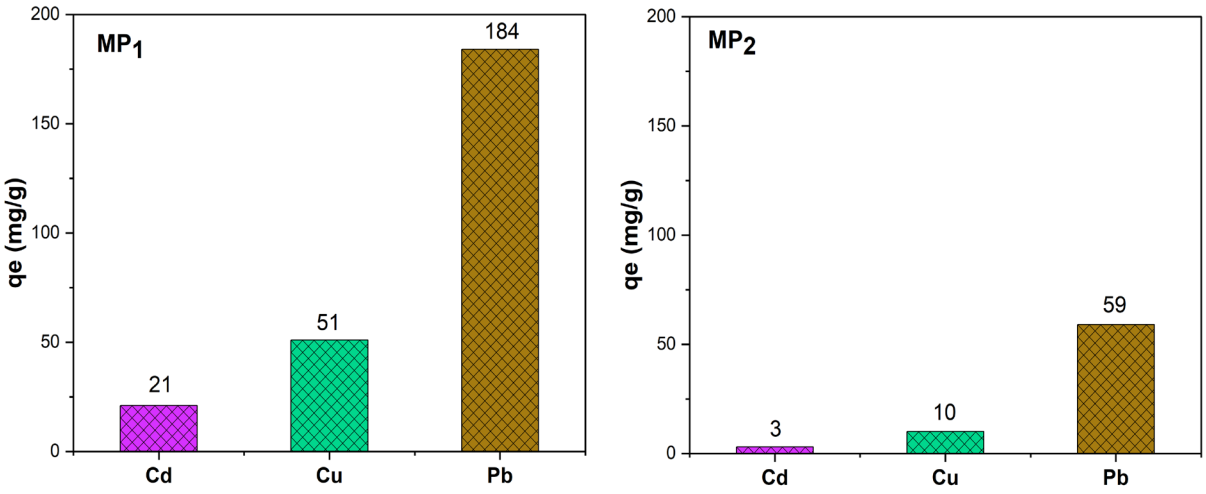

Figure 9. Effect of the presence of other metal ions on the adsorption efficiency of **MP1** (left) and **MP2** (right) to extract Pb(II) ion: Adsorption conditions: 10 mg of each adsorbent in 10 mL of an aqueous solution containing Cd(II), Cu(II) and Pb(II) ions at the optimal concentration for Pb(II) at pH 6.0 and 298 K for 45 min

2.3.6. Reusability of the adsorbents

Silica-based materials, including those incorporating porphyrins, are known for their ability to be regenerated and reused without significant performance loss, as reported in the literature.[71,25]

To assess the impact of **MCM-41** on the reusability of **MP1** and **MP2** for extracting Cd(II), Cu(II), and Pb(II) ions, their regeneration capacity was analyzed over five cycles. In these assays, after each adsorption process, the fully loaded materials were treated with 4 % nitric acid under

mechanical stirring for 2 h. The solids were then thoroughly washed with water until the filtrate reached a neutral pH and the process was repeated five times.

The results presented Figure 10, confirm that both materials maintained excellent adsorption efficiency for each metal ion, even after five consecutive uses. **MP1** and **MP2** lost less than 4 % and 10 %, respectively in Pb(II) extraction, demonstrating their suitability for multiple usage.[72] The minor decrease in the adsorption capacity may result from the retention of metal ions in coordinative sites that were not removed under acidic conditions or from their protonation. It is also important to note that analysis of the 4 % nitric acid filtrate by UV-vis spectroscopy showed no Soret or Q-band signatures of free porphyrins. This confirms the environmental safety of the materials, as no porphyrin release was detected during the washing and regeneration process. The slight loss in efficiency is likely due to a combination of incomplete metal ion removal and partial protonation of the free-nitrogen sites.

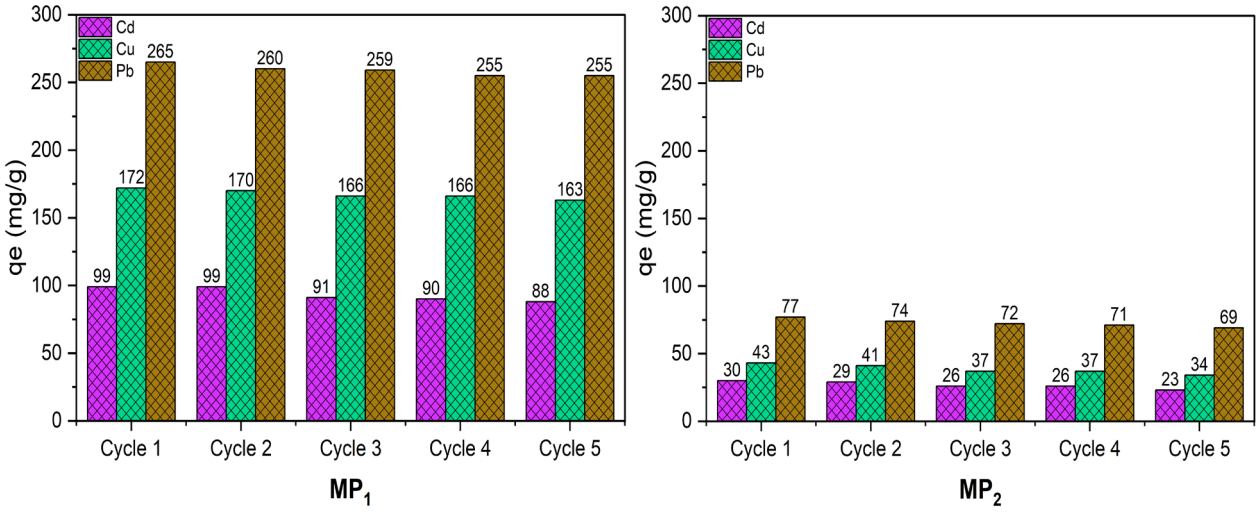

Figure 10. Regeneration performance of **MP1** (right) and **MP2** (left) over five cycles of metals extractions. Under the adsorption conditions of 10 mg adsorbents in 10 mL of an aqueous solution containing metal ion at its optimal concentration, at pH 6.0 and 298 K for 45 min. After each cycle the material was recovered after acidic treatment and reused.

2.3.7. Application in real world contaminated water

Removing trace amounts of hazardous metal ions from real contaminated water is particularly challenging, not only because other competing cations may interfere with the

adsorption process, but also because organic matter commonly found in natural water can hinder adsorption. That is why one of the most valuable qualities in an adsorbent is its ability to remain effective even at low metal ion concentrations.

The Marchica River, located in Nador, Morocco, has long been affected by various pollutants, including both organic and inorganic wastes.[14] Despite numerous efforts and projects to purify the river, heavy metals remain a significant concern, as they are difficult to remove completely at low concentrations. In this study, we collected water samples from the river and tested our newly developed hybrid materials to evaluate their effectiveness in real-world conditions. This assessment was conducted in the presence of other potential cationic elements to simulate practical application scenarios. Table 8 shows the concentration of metal ions found in the samples retrieved from Marchica, as well as the extracted values using **MP_1** and **MP_2.**

Both materials displayed effective performance in extracting their target metal ions from the Marchica River with **MP_1** achieving 89 % removal and **MP_2** 55 %. Notably, **MP_1** removed 89 % of Pb(II) ion even at low concentrations, reducing it to just 0.36 mg/L, well below hazardous levels. **MP_1** also demonstrated strong efficiency in Cu(II) ion removal, achieving 74 % adsorption.

On the other hand, Table 9 presents the amount of metal ions removed by **MP_1** and **MP_2** from a Marchica water sample spiked to a concentration of 180 mg/L for each metal ion. Despite the elevated concentration, both materials showed promising performance, with **MP_1** standing out by achieving a 65% removal rate. This demonstrates their practical effectiveness not only at trace levels but also under more demanding, high-concentration conditions.

These results confirm the reliability of these materials in real-world contaminated samples, even in the presence of competing cations. Their high adsorption capacity, fast and selective removal, and reusability make them a cost-effective solution for lead remediation. **MP_1**, with its superior performance, stands out as the more effective option.

Table 8. Concentration of metal ions found and the amount removed by **MP_1** and **MP_2** using optimal experimental conditions (298 K for 45 min).

Adsorbent	Metal	Concentration (mg/L)		%
		Found	Removed	Removed
MP_1	Cd(II)	3.01	1.00	33%
	Cu(II)	15.17	11.17	74%
	Pb(II)	3.27	2.91	89%

MP₂	Cd(II)	3.01	0.02	0.7%
	Cu(II)	15.17	4.08	27%
	Pb(II)	3.27	1.80	55%

Table 9. Amount of metal ions removed by **MP₁** and **MP₂** from Marchika water, initially loaded with 180 mg/L of each metal ion, under optimized conditions (298 K, 45 min.).

Adsorbent	Metal	Concentration (mg/L)		%
		Found	Removed	Removed
MP₁	Cd(II)	180	11.24	6%
	Cu(II)	180	22.36	12%
	Pb(II)	180	116.74	65%
MP₂	Cd(II)	180	5.36	3%
	Cu(II)	180	10.65	6%
	Pb(II)	180	47.37	26%

2.3.8. Comparative evaluation of Pb(II) adsorption capacity of **MP₁** and **MP₂** with other adsorbents

In Table 10 are summarized the results obtained with other adsorbents reported in literature, which also showed high efficiency for Pb(II), alongside with the results obtained with **MP₁** and **MP₂**. This analysis allows evaluating the impact of the attaching porphyrinic ligands to **MCM-41** on their adsorption properties.

The results show that **MP₁** demonstrates a highly competitive performance, namely when compared with porphyrinic ligands immobilized in conventional silica. **MP₁** surpasses most reported materials in terms of efficiency, selectivity, and rapid adsorption. Finding comparable materials was challenging, leading us to extend the comparison to different material classes, where **MP₁** still performed exceptionally well. For example, while graphene oxide (GO-HPEI gel) achieved a higher overall adsorption capacity, it required over 6 h to reach saturation, whereas **MP₁** and **MP₂** achieved their maximum adsorption in about 45 min. Additionally, cross-linked graphene oxide materials are significantly more complex to synthesize compared to our adsorbents. The combination of high efficiency, fast kinetics, and straightforward synthesis makes these newly developed hybrid materials particularly advantageous, outperforming many well-established adsorbents for Pb(II) removal.

Table 10. Comparative study of Pb(II) ion extraction capacity of the new hybrid materials **MP_1** and **MP_2** and those found with the literature.

Adsorbent	Adsorption capacity of Pb(II) ion (mg/g)	Efficiency after reusability	References
MP_1	265.70	~96% after 5 cycles	This work
MP_2	77.69	~90% after 5 cycles	This work
βCD-AC-CaBent	39.78	~97% after 3 cycles	[73]
SiNPz	94.18	Not specified	[74]
SiNPz-Th	102.27	~98% after 5 cycles	[75]
SiNPz-Py	110.84	~98% after 5 cycles	[76]
Bio-hybrid silsesquioxane/yeast	248.00	N/A	[77]
CJA	175.16	~87% after 7 cycles	[78]
GO-HPEI gel	438.60	~89% after 8 cycles	[79]
Silica-MPTMS	186.06	N/A	[80]
PMAEEDA	61.90	~80 after 9 cycles	[81]
MCM-41-DETA	192.90	N/A	[82]
$SiTPF_5PP$	187.07	Not Specified	[33]

N/A: Not applicable

3. Experimental section

3.1. Materials

All experiments were conducted using double-distilled water with a conductivity of ≤1.5 µS/cm. Stock solutions of metal ions were prepared from commercially available metal salts: $Cd(NO_3)_2 \cdot 6H_2O$, $Cu(NO_3)_2 \cdot 3H_2O$, and $Pb(NO_3)_2 \cdot 6H_2O$. All solvents used were of analytical grade, with a purity exceeding 99.5 %, and were used without further purification unless drying was required, following standard protocols. Commercial **MCM-41** with a hexagonal pore structure and a pore volume of 0.98 cm^3/g was activated in an oven at 120 °C for 12 h prior utilization as a support for synthesizing hybrid adsorbents **MP_1** and **MP_2**. The porphyrin ligands **P_1** and **P_2** were synthesized using well-established methods documented in the literature.[44,83] For real-world testing, contaminated water samples were collected from the Marchica River in Nador, Morocco, at GPS coordinates 535Q+WGR.

3.2. MCM-41 Based adsorbents preparation

3.2.1. Synthesis of **MCM-41- NH_2** and **MCM-41-Cl**

The synthesis of functionalized **MCM-41-NH_2** and **MCM-41-Cl** was carried out according to the documented procedure.[40] In a 250 mL two-neck flask, 2 g of previously activated **MCM-41** was suspended in 80 mL of dry toluene under a nitrogen atmosphere. To this, 1 mL of APTMS or CPTMS were added, and the mixture was refluxed for 2 h. Afterward, 5 mL of toluene was distilled off, followed by the addition of 2 mL of APTMS or CPTMS. This cycle was repeated three times, with the final addition consisting of 4 mL of silane agents. The reaction was allowed to proceed for 48 h before the resulting solid was collected by filtration. The materials were sequentially washed—first with 5 mL of toluene, then with methanol, and finally with dichloromethane. The purified product was then dried in an oven at 50 °C for 6 h, yielding the functionalized **MCM-41-NH_2** and **MCM-41-Cl**.

3.2.2. Synthesis of **MP_1**

A mixture containing 2 g of **MCM41-NH_2** previously synthesized and 150 mg of 5,10,15,20-tetrakis(pentafluorophenyl)porphyrin (**P_1**) in 30 mL of dry toluene was maintained under reflux (110 °C) for 48 h under nitrogen atmosphere. Then, the resulting solid was filtered, washed with toluene, methanol and dichloromethane three times each and then dried in an oven at 60 °C for 12 h to obtain the material **MP_1**.

3.2.3. Synthesis of **MP_2**

A mixture containing 2 g of **MCM41-Cl** previously synthesized and 150 mg of 5,10,15,20-tetra(pyridin-4-yl)porphyrin (**P_2**) in 20 mL of *o*-dichlorobenzene was maintained under reflux (180 °C) for 48 h under nitrogen atmosphere. Then, the resulting mixture was centrifugated and washed several times with a mixture of dichloromethane and methanol (9:1) until the solution centrifugated was colorless. The solid was dried in an oven at 60 °C for 12 h to obtain the material **MP_2**.

3.3. Metal ions adsorption study

The adsorption experiments for metal ions using the newly synthesized adsorbents, **MP_1** and **MP_2**, were carried out in batch mode. Each test was performed three times, and the average result was recorded. After the adsorption process, the solid phase was separated by filtration using

a 0.45 mm syringe filter. The remaining metal ion concentration in the filtrate was then measured using an atomic absorption spectrophotometer.

The adsorption capacity of each hybrid for Cd(II), Cu(II), and Pb(II) was determined using the following equation:

$$q_e = (C_0 - C_e)\frac{V}{m}$$

Where, q_e represents the amount of each metal ion on the adsorbent (mg/g), C_0 and C_e are the initial concentration and equilibrium concentration in solution respectively (mg/L), V is the volume of metallic solution (L), and m is the weight of the adsorbents (g).

The effect of each parameter on the adsorption capacity of **MP_1** and **MP_2** was assessed separately using the following approach:

Effect of Initial Concentration: To assess the influence of initial metal ion concentration, 10 mL of solutions containing Cd(II), Cu(II), and Pb(II) ions at varying concentrations (e.g. 50, 80, 110, 140, 170, 200, 250, 300, 350, 400, 450, and 500 mg/L) were added to conical flasks containing 10 mg of either **MP_1** or **MP_2**. The mixtures were stirred for 2 h at 298 K, with the pH fixed at 6.0. Metal ion concentrations in the filtrate were then analyzed as described previously. Based on this experiment, the optimal concentrations were determined and summarized in Table 10.

Table 11. Metal ion's optimal concentration for **MP_1** and **MP_2**.

Material	Metal ion	Optimal concentration (mg/L)
MP_1	Cd(II)	195
	Cu(II)	270
	Pb(II)	370
MP_2	Cd(II)	130
	Cu(II)	180
	Pb(II)	210

Effect of Contact Time: To determine the optimal contact time, 10 mg of each hybrid material was introduced into a conical flask, followed by 10 mL of metal ion's optimal concentration solution. The concentration of remaining metal ions in the filtrate was measured at different time

intervals: 5, 10, 15, 20, 25, 30, 45, and 60 min. All tests were conducted at 298 K and pH 6.0. The results indicated that adsorption reached its peak efficiency at 45 min.

Thermodynamic Study: To evaluate the thermodynamic behavior of adsorption, 10 mg of each adsorbent was mixed with 10 mL of the metal ion's optimal concentration solution. The experiment was conducted at three different temperatures (298 K, 308 K, and 318 K), while keeping all other parameters at their optimal values (contact time: 45 min, pH: 6.0). Metal ion concentrations in the filtrate were then analyzed.

Effect of pH Variation: To study the influence of pH, 10 mg of each adsorbent was added to 10 mL of metal ion's optimal concentration solution with pH adjusted to 3, 4, 5, 6 and 7. The samples were stirred for 45 min at 298 K, and metal ion concentrations were measured in the filtrate. pH adjustments were made using diluted HCl and NaOH solutions. The optimal pH for adsorption was determined to be 6.0.

Selectivity Study: To investigate selectivity, 10 mg of each adsorbent was introduced into a conical flask containing a mixture of Cd(II), Cu(II) and Pb(II) ions, each at 370 mg/g for **MP_1** and 210 mg/g for **MP_2** in 10 mL of solution. The samples were stirred for 45 min at 298 K and pH 6.0, and the concentrations of metal ions in the filtrate were analyzed to determine the selectivity of each material.

Reusability Assessment: To evaluate the reusability of the adsorbents, 1 g of each metal-loaded material was placed in 10 mL of 4 % nitric acid and stirred for 2 h. After filtration, the solid was washed with water until the filtrate's pH was neutral, then dried. After, 10 mg of the regenerated material was reused for adsorption, and this process was repeated 5 times. The adsorption efficiency after each cycle was recorded.

Real Water Decontamination: For real-world application testing, 10 mL of water samples from the Marchica River were introduced into conical flasks containing 10 mg of adsorbent. After 45 min of contact at 298 K, metal ion concentrations in the filtrate were analyzed.

4. Conclusion

In this study, we successfully synthesized and characterized two novel hybrid materials, **MP_1** and **MP_2**, by modifying MCM-41 with two types of porphyrin molecules. Comprehensive characterization confirmed successful functionalization, ensuring their structural integrity and adsorption capabilities.

As a new concept, we integrate porphyrinic N-donor sites into an accessible mesoporous MCM-41 scaffold to promote inner-sphere Metal–N complexation and mesopore-confined mass transfer. This affords a simple and scalable silica platform that couples high capacity, rapid uptake, selectivity, and reusability. Importantly, this work introduces a single hybrid adsorbent that bridges advantages across all key adsorption parameters—combining high capacity, fast kinetics, strong selectivity under competition, favorable thermodynamics (spontaneous/endothermic), robust reusability, and proven efficacy in real river water—within one system.

Both materials demonstrated effective performance in heavy metal ion adsorption, particularly for Pb(II) ion. **MP_1** and **MP_2** achieved maximum adsorption capacities of 265.7 mg/g and 77.7 mg/g towards Pb(II) ion respectively, comparing favorably to existing materials. Their adsorption kinetics were remarkably fast, with 65 % of Pb(II) ion removed within just 10 min and complete adsorption within 45 min. Thermodynamic analysis further confirmed that the adsorption process is spontaneous and efficient at ambient temperature, demonstrating their practicality for industrial applications.

Besides capacity and rate, **MP_1** and **MP_2** exhibited outstanding selectivity, removing 70 % of Pb(II) ion even in the presence of competing ions at equal concentrations. Their reusability was also confirmed, with minimal efficiency loss, less than 4 % for **MP_1** and 10 % for **MP_2**, after five consecutive cycles. Most importantly, these materials proved highly reliable in real-world conditions, achieving 89 % and 55 % Pb(II) ion removal from contaminated water samples from the Marchica River, even at trace lead concentrations.

Compared with related work, the MCM-41/porphyrin design outperforms the same porphyrin on conventional silica (≈42% higher Pb(II) capacity; 265.7 vs 187.4 mg g^{-1}) and rivals more complex adsorbents while reaching equilibrium in ~45 min, whereas many high-capacity systems require multi-hour contact times. Thus, the combination of high efficiency, rapid adsorption, strong selectivity, durability, and real-world applicability makes **MP_1** a promising material for heavy metal remediation, particularly for lead-contaminated water treatment.

Authors Contributions

Youssef Draoui: Investigation, Conceptualization, Writing – original draft, Writing – review and editing. Smaail Radi: Methodology, Supervision, Writing – review and editing. Mengmeng Wang: Investigation, editing. Amal El Mahdaoui: Investigation. Chahrazad El Abiad: Validation, Writing.

Aurelian Rotaru: Investigation, Resources. Yann Garcia: Investigation, Resources, Writing – review and editing. M. Amparo F. Faustino: Validation, Writing – review and editing. M. Graça P. M. S. Neves: Methodology, Validation, Writing – review and editing. Nuno M. M. Moura: Methodology, Conceptualization, Supervision, Writing – review and editing.

Funding

This research work received financial support from the University of Aveiro and FCT/MCTES (Fundação para a Ciência e Tecnologia and Ministério da Ciência, Tecnologia e Ensino Superior) to support the Laboratório Associado para a Química Verde - Tecnologias e Processos Limpos (LAQV-REQUIMTE; UID/50006) research unit through national funds and, where applicable, was co-financed by the FEDER, within the PT2020 Partnership Agreement, and to the Portuguese NMR Network. NMR spectrometers are part of the National NMR Network (PTNMR) and are partially supported by Infrastructure Project Nº 022161 (co-financed by FEDER through COMPETE 2020, POCI and PORL and FCT through PIDDAC). N.M.M. Moura gratefully acknowledges FCT for an Assistant Research Position thanks under the Individual Scientific Employment Stimulus - 6th Edition (2023.06495.CEECIND/CP2840/CT0031; DOI: 10.54499/2023.06495.CEECIND/CP2840/CT0031). Y. Draoui thanks the Erasmus program for the exchange mobility between Morocco and Portugal.

Acknowledgements

The authors thank the University of Aveiro and FCT/MCTES for financial support to LAQV-REQUIMTE (LA/P/0008/2020, and UIDP/50006/2020 and UIDB/50006/2020) research units, and Portuguese NMR Network. “The NMR spectrometers are part of the National NMR Network (PTNMR) and are partially supported by Infrastructure Project Nº 022161 (co-financed by FEDER through COMPETE 2020, POCI and PORL and FCT through PIDDAC). The authors extend their appreciation to the European Union Program Erasmus+ ICM Project (Ref. 2020-1-PT01KA107-077895) for financial support.

Notes

The authors declare no competing financial interest.

References

(1) Nag, R.; Cummins, E. Human Health Risk Assessment of Lead (Pb) through the Environmental-Food Pathway. *Science of The Total Environment* **2022**, *810*, 151168. https://doi.org/10.1016/j.scitotenv.2021.151168.

(2) Levin, R.; Zilli Vieira, C. L.; Rosenbaum, M. H.; Bischoff, K.; Mordarski, D. C.; Brown, M. J. The Urban Lead (Pb) Burden in Humans, Animals and the Natural Environment. *Environmental Research* **2021**, *193*, 110377. https://doi.org/10.1016/j.envres.2020.110377.

(3) Boskabady, M.; Marefati, N.; Farkhondeh, T.; Shakeri, F.; Farshbaf, A.; Boskabady, M. H. The Effect of Environmental Lead Exposure on Human Health and the Contribution of Inflammatory Mechanisms, a Review. *Environment International* **2018**, *120*, 404–420. https://doi.org/10.1016/j.envint.2018.08.013.

(4) Liu, W.; Tian, J.; Chen, L.; Guo, Y. Temporal and Spatial Characteristics of Lead Emissions from the Lead-Acid Battery Manufacturing Industry in China. *Environmental Pollution* **2017**, *220*, 696–703. https://doi.org/10.1016/j.envpol.2016.10.031.

(5) Besser, J. M.; Brumbaugh, W. G.; Allert, A. L.; Poulton, B. C.; Schmitt, C. J.; Ingersoll, C. G. Ecological Impacts of Lead Mining on Ozark Streams: Toxicity of Sediment and Pore Water. *Ecotoxicology and Environmental Safety* **2009**, *72* (2), 516–526. https://doi.org/10.1016/j.ecoenv.2008.05.013.

(6) O'Connor, D.; Hou, D.; Ye, J.; Zhang, Y.; Ok, Y. S.; Song, Y.; Coulon, F.; Peng, T.; Tian, L. Lead-Based Paint Remains a Major Public Health Concern: A Critical Review of Global Production, Trade, Use, Exposure, Health Risk, and Implications. *Environment International* **2018**, *121*, 85–101. https://doi.org/10.1016/j.envint.2018.08.052.

(7) Bindler, R. Contaminated Lead Environments of Man: Reviewing the Lead Isotopic Evidence in Sediments, Peat, and Soils for the Temporal and Spatial Patterns of Atmospheric Lead Pollution in Sweden. *Environ Geochem Health* **2011**, *33* (4), 311–329. https://doi.org/10.1007/s10653-011-9381-7.

(8) Araki, S.; Sato, H.; Yokoyama, K.; Murata, K. Subclinical Neurophysiological Effects of Lead: A Review on Peripheral, Central, and Autonomic Nervous System Effects in Lead Workers. *American journal of industrial medicine* **2000**, *37* (2), 193–204.

(9) Ramírez Ortega, D.; González Esquivel, D. F.; Blanco Ayala, T.; Pineda, B.; Gómez Manzo, S.; Marcial Quino, J.; Carrillo Mora, P.; Pérez De La Cruz, V. Cognitive Impairment Induced

by Lead Exposure during Lifespan: Mechanisms of Lead Neurotoxicity. *Toxics* **2021**, *9* (2), 23. https://doi.org/10.3390/toxics9020023.

(10) Harari, F.; Sallsten, G.; Christensson, A.; Petkovic, M.; Hedblad, B.; Forsgard, N.; Melander, O.; Nilsson, P. M.; Borné, Y.; Engström, G.; Barregard, L. Blood Lead Levels and Decreased Kidney Function in a Population-Based Cohort. *American Journal of Kidney Diseases* **2018**, *72* (3), 381–389. https://doi.org/10.1053/j.ajkd.2018.02.358.

(11) Navas-Acien, A.; Guallar, E.; Silbergeld, E. K.; Rothenberg, S. J. Lead Exposure and Cardiovascular Disease—A Systematic Review. *Environ Health Perspect* **2007**, *115* (3), 472–482. https://doi.org/10.1289/ehp.9785.

(12) Kumar, S. R.; Devi, Asha. S. Lead Toxicity on Male Reproductive System and Its Mechanism: A Review. *Rese. Jour. of Pharm. and Technol.* **2018**, *11* (3), 1228. https://doi.org/10.5958/0974-360X.2018.00228.7.

(13) Organization, W. H. Lead in Drinking-Water: Health Risks, Monitoring and Corrective Actions: Technical Brief. In *Lead in drinking-water: health risks, monitoring and corrective actions: technical brief*; 2022.

(14) Aknaf, A.; Akodad, M.; Layachi, M.; Baghour, M.; Oudra, B.; Vasconcelos, V. The Chemical Characterization and Its Relationship with Heavy Metals Contamination in Surface Sediment of Marchica Mediterranean Lagoon (North of Morocco). *Environ Sci Pollut Res* **2022**, *29* (3), 4159–4169. https://doi.org/10.1007/s11356-021-15641-4.

(15) Qasem, N. A. A.; Mohammed, R. H.; Lawal, D. U. Removal of Heavy Metal Ions from Wastewater: A Comprehensive and Critical Review. *npj Clean Water* **2021**, *4* (1), 36. https://doi.org/10.1038/s41545-021-00127-0.

(16) Zamora-Ledezma, C.; Negrete-Bolagay, D.; Figueroa, F.; Zamora-Ledezma, E.; Ni, M.; Alexis, F.; Guerrero, V. H. Heavy Metal Water Pollution: A Fresh Look about Hazards, Novel and Conventional Remediation Methods. *Environmental Technology & Innovation* **2021**, *22*, 101504. https://doi.org/10.1016/j.eti.2021.101504.

(17) Fu, F.; Wang, Q. Removal of Heavy Metal Ions from Wastewaters: A Review. *Journal of Environmental Management* **2011**, *92* (3), 407–418. https://doi.org/10.1016/j.jenvman.2010.11.011.

(18) Hossain, M. S.; Shenashen, M. A.; Awual, M. E.; Rehan, A. I.; Rasee, A. I.; Waliullah, R. M.; Kubra, K. T.; Salman, Md. S.; Sheikh, Md. C.; Hasan, Md. N.; Hasan, Md. M.; Islam, A.;

Khaleque, Md. A.; Marwani, H. M.; Alzahrani, K. A.; Asiri, A. M.; Rahman, M. M.; Awual, Md. R. Benign Separation, Adsorption, and Recovery of Rare-Earth Yb(III) Ions with Specific Ligand-Based Composite Adsorbent. *Process Safety and Environmental Protection* **2024**, *185*, 367–374. https://doi.org/10.1016/j.psep.2024.03.026.

(19) Salman, Md. S.; Znad, H.; Hasan, Md. N.; Hasan, Md. M. Optimization of Innovative Composite Sensor for Pb(II) Detection and Capturing from Water Samples. *Microchemical Journal* **2021**, *160*, 105765. https://doi.org/10.1016/j.microc.2020.105765.

(20) Rajendran, S.; Priya, A. K.; Senthil Kumar, P.; Hoang, T. K. A.; Sekar, K.; Chong, K. Y.; Khoo, K. S.; Ng, H. S.; Show, P. L. A Critical and Recent Developments on Adsorption Technique for Removal of Heavy Metals from Wastewater-A Review. *Chemosphere* **2022**, *303*, 135146. https://doi.org/10.1016/j.chemosphere.2022.135146.

(21) Saccullo, E.; Patamia, V.; Magaletti, F.; Dativo, G.; Camarda, M.; Fiorenza, R.; Barbera, V.; Floresta, G.; Rescifina, A. Halloysite-Kojic Acid Conjugate: A Sustainable Material for the Photocatalytic CO2 Reduction and Fixation for Cyclic Carbonates Production. *Journal of CO2 Utilization* **2024**, *85*, 102865. https://doi.org/10.1016/j.jcou.2024.102865.

(22) Saccullo, E.; Dativo, G.; Lombardo, R.; Armeli Iapichino, M. T.; Fiorenza, R.; Patamia, V.; Floresta, G. Natural Antenna Molecule in Halloysite-Kojic Acid Composite for the Solar Photocatalytic CO2 Methanation. *Materials Today Chemistry* **2025**, *44*, 102587. https://doi.org/10.1016/j.mtchem.2025.102587.

(23) Ferlazzo, A.; Armeli Iapichino, M. T.; Calabrese, G.; D'Accurso, G.; Fiorenza, R.; Pistarà, V.; Gulino, A.; Rescifina, A.; Patamia, V.; Floresta, G. Nanosensors Made of Halloysite and Kojic Acid Metal Complexes for Dopamine Detection. *ACS Appl. Nano Mater.* **2025**, *8* (34), 16736–16747. https://doi.org/10.1021/acsanm.5c02759.

(24) Radi, S.; Tighadouini, S.; Toubi, Y.; Bacquet, M. Polysiloxane Surface Modified with Bipyrazolic Tripodal Receptor for Quantitative Lead Adsorption. *Journal of Hazardous Materials* **2011**, *185* (1), 494–501. https://doi.org/10.1016/j.jhazmat.2010.09.016.

(25) El Abiad, C.; Radi, S.; El Massaoudi, M.; Lamsayah, M.; Figueira, F.; Faustino, M. A. F.; Neves, M. G. P. M. S.; Moura, N. M. M. Porphyrin-Silica Gel Hybrids as Effective and Selective Copper(II) Adsorbents from Industrial Wastewater. *Journal of Environmental Chemical Engineering* **2023**, *11* (3), 110097. https://doi.org/10.1016/j.jece.2023.110097.

(26) Radi, S.; El Abiad, C.; Carvalho, A. P.; Santos, S. M.; Faustino, M. A. F.; Neves, M. G. P. M. S.; Moura, N. M. M. An Efficient Hybrid Adsorbent Based on Silica-Supported Amino Penta-Carboxylic Acid for Water Purification. *J. Mater. Chem. A* **2018**, *6* (27), 13096–13109. https://doi.org/10.1039/C8TA02560F.

(27) Kubra, K. T.; Hasan, Md. M.; Hasan, Md. N.; Salman, Md. S.; Khaleque, Md. A.; Sheikh, Md. C.; Rehan, A. I.; Rasee, A. I.; Waliullah, R. M.; Awual, M. E.; Hossain, M. S.; Alsukaibi, A. K. D.; Alshammari, H. M.; Awual, Md. R. The Heavy Lanthanide of Thulium(III) Separation and Recovery Using Specific Ligand-Based Facial Composite Adsorbent. *Colloids and Surfaces A: Physicochemical and Engineering Aspects* **2023**, *667*, 131415. https://doi.org/10.1016/j.colsurfa.2023.131415.

(28) Tighadouini, S.; Radi, S.; Elidrissi, A.; Haboubi, K.; Bacquet, M.; Degoutin, S.; Zaghrioui, M.; Garcia, Y. Removal of Toxic Heavy Metals from River Water Samples Using a Porous Silica Surface Modified with a New β-Ketoenolic Host. *Beilstein J. Nanotechnol.* **2019**, *10*, 262–273. https://doi.org/10.3762/bjnano.10.25.

(29) El-Massaoudi, M.; Radi, S.; Lamsayah, M.; Tighadouini, S.; Séraphin, K. K.; Kouassi, L. K.; Garcia, Y. Ultra-Fast and Highly Efficient Hybrid Material Removes Cu(II) from Wastewater: Kinetic Study and Mechanism. *Journal of Cleaner Production* **2021**, *284*, 124757. https://doi.org/10.1016/j.jclepro.2020.124757.

(30) Radi, S.; Toubi, Y.; El-Massaoudi, M.; Bacquet, M.; Degoutin, S.; Mabkhot, Y. N. Efficient Extraction of Heavy Metals from Aqueous Solution by Novel Hybrid Material Based on Silica Particles Bearing New Schiff Base Receptor. *Journal of Molecular Liquids* **2016**, *223*, 112–118. https://doi.org/10.1016/j.molliq.2016.08.024.

(31) Khaled, R. K.; Wahba, M. A.; Badry, M. D.; Zawrah, M. F.; Heikal, E. A. Highly Ordered Pure and Indium-Incorporated MCM-41 Mesoporous Adsorbents: Synthesis, Characterization and Evaluation for Dye Removal. *J Mater Sci* **2022**, *57* (7), 4504–4527. https://doi.org/10.1007/s10853-022-06877-7.

(32) Chen, H.; Wang, Y. Preparation of MCM-41 with High Thermal Stability and Complementary Textural Porosity. *Ceramics International* **2002**, *28* (5), 541–547. https://doi.org/10.1016/S0272-8842(02)00007-X.

(33) El Abiad, C.; Radi, S.; Faustino, M.; Neves, M.; Moura, N. Supramolecular Hybrid Material Based on Engineering Porphyrin Hosts for an Efficient Elimination of Lead(II) from Aquatic Medium. *Molecules* **2019**, *24* (4), 669. https://doi.org/10.3390/molecules24040669.

(34) Li, S.; Wang, L.; Lu, P.; Li, Y.; Li, Y.; Wang, Y.; Yao, L.; Qiu, D. Nanoconfined Polyethyleneimine in Mesoporous MCM-41 Silica for Heavy Metal Ions Removal. *Separation and Purification Technology* **2025**, *353*, 128421. https://doi.org/10.1016/j.seppur.2024.128421.

(35) Kruk, M.; Jaroniec, M.; Sayari, A. Application of Large Pore MCM-41 Molecular Sieves To Improve Pore Size Analysis Using Nitrogen Adsorption Measurements. *Langmuir* **1997**, *13* (23), 6267–6273. https://doi.org/10.1021/la970776m.

(36) Chen, L. Y.; Jaenicke, S.; Chuah, G. K. Thermal and Hydrothermal Stability of Framework-Substituted MCM-41 Mesoporous Materials. *Microporous Materials* **1997**, *12* (4–6), 323–330. https://doi.org/10.1016/S0927-6513(97)00079-5.

(37) Pyrzynska, K.; Kilian, K. Porphyrin-Based Sorbents for the Enrichment and Removal of Metal Ions. *Molecules* **2025**, *30* (10), 2238. https://doi.org/10.3390/molecules30102238.

(38) Vallejo, M. C. S.; Reis, M. J. A.; Pereira, A. M. V. M.; Serra, V. V.; Cavaleiro, J. A. S.; Moura, N. M. M.; Neves, M. G. P. M. S. Merging Pyridine(s) with Porphyrins and Analogues: An Overview of Synthetic Approaches. *Dyes and Pigments* **2021**, *191*, 109298. https://doi.org/10.1016/j.dyepig.2021.109298.

(39) Bayuo, J.; Rwiza, M. J.; Choi, J. W.; Mtei, K. M.; Hosseini-Bandegharaei, A.; Sillanpää, M. Adsorption and Desorption Processes of Toxic Heavy Metals, Regeneration and Reusability of Spent Adsorbents: Economic and Environmental Sustainability Approach. *Advances in Colloid and Interface Science* **2024**, *329*, 103196. https://doi.org/10.1016/j.cis.2024.103196.

(40) De Lima, A. L.; Mbengue, A.; San Gil, R. A. S.; Ronconi, C. M.; Mota, C. J. A. Synthesis of Amine-Functionalized Mesoporous Silica Basic Catalysts for Biodiesel Production. *Catalysis Today* **2014**, *226*, 210–216. https://doi.org/10.1016/j.cattod.2014.01.017.

(41) Adler, A. D.; Longo, F. R.; Finarelli, J. D.; Goldmacher, J.; Assour, J.; Korsakoff, L. A Simplified Synthesis for Meso-Tetraphenylporphine. *J. Org. Chem.* **1967**, *32* (2), 476–476. https://doi.org/10.1021/jo01288a053.

(42) Gonsalves, A. M. d'A R.; Varejão, J. M. T. B.; Pereira, M. M. Some New Aspects Related to the Synthesis of *Meso* -substituted Porphyrins. *Journal of Heterocyclic Chem* **1991**, *28* (3), 635–640. https://doi.org/10.1002/jhet.5570280317.

(43) Lindsey, J. S.; Schreiman, I. C.; Hsu, H. C.; Kearney, P. C.; Marguerettaz, A. M. Rothemund and Adler-Longo Reactions Revisited: Synthesis of Tetraphenylporphyrins under Equilibrium Conditions. *J. Org. Chem.* **1987**, *52* (5), 827–836. https://doi.org/10.1021/jo00381a022.

(44) Costa, J. I. T.; Tomé, A. C.; Neves, M. G. P. M. S.; Cavaleiro, J. A. S. 5,10,15,20-Tetrakis(Pentafluorophenyl)Porphyrin: A Versatile Platform to Novel Porphyrinic Materials. *J. Porphyrins Phthalocyanines* **2011**, *15* (11n12), 1116–1133. https://doi.org/10.1142/S1088424611004294.

(45) Mutneja, R.; Singh, R.; Kaur, V.; Wagler, J.; Fels, S.; Kroke, E. Schiff Base Tailed Silatranes for the Fabrication of Functionalized Silica Based Magnetic Nano-Cores Possessing Active Sites for the Adsorption of Copper Ions. *New J. Chem.* **2016**, *40* (2), 1640–1648. https://doi.org/10.1039/C5NJ02287H.

(46) Şen, P.; Hirel, C.; Andraud, C.; Aronica, C.; Bretonnière, Y.; Mohammed, A.; Ågren, H.; Minaev, B.; Minaeva, V.; Baryshnikov, G.; Lee, H.-H.; Duboisset, J.; Lindgren, M. Fluorescence and FTIR Spectra Analysis of Trans-A2B2-Substituted Di- and Tetra-Phenyl Porphyrins. *Materials* **2010**, *3* (8), 4446–4475. https://doi.org/10.3390/ma3084446.

(47) Arakaki, L. N. H.; Filha, V. L. S. A.; Germano, A. F. S.; Santos, S. S. G.; Fonseca, M. G.; Sousa, K. S.; Espínola, J. G. P.; Arakaki, T. Silica Gel Modified with Ethylenediamine and Succinic Acid-Adsorption and Calorimetry of Cations in Aqueous Solution. *Thermochimica Acta* **2013**, *556*, 34–40. https://doi.org/10.1016/j.tca.2013.01.024.

(48) Pérez-Quintanilla, D.; Sánchez, A.; Del Hierro, I.; Fajardo, M.; Sierra, I. Preparation, Characterization, and Zn2+ Adsorption Behavior of Chemically Modified MCM-41 with 5-Mercapto-1-Methyltetrazole. *Journal of Colloid and Interface Science* **2007**, *313* (2), 551–562. https://doi.org/10.1016/j.jcis.2007.04.063.

(49) Zhang, Y.; Qu, R.; Sun, C.; Wang, C.; Ji, C.; Chen, H.; Yin, P. Chemical Modification of Silica-Gel with Diethylenetriamine via an End-Group Protection Approach for Adsorption to Hg(II). *Applied Surface Science* **2009**, *255* (11), 5818–5826. https://doi.org/10.1016/j.apsusc.2009.01.011.

(50) Thommes, M.; Kaneko, K.; Neimark, A. V.; Olivier, J. P.; Rodriguez-Reinoso, F.; Rouquerol, J.; Sing, K. S. W. Physisorption of Gases, with Special Reference to the Evaluation of Surface Area and Pore Size Distribution (IUPAC Technical Report). *Pure and Applied Chemistry* **2015**, *87* (9–10), 1051–1069. https://doi.org/10.1515/pac-2014-1117.

(51) Yan, B.; Li, Y.; Zhou, B. Covalently Bonding Assembly and Photophysical Properties of Luminescent Molecular Hybrids Eu–TTA–Si and Eu–TTASi–MCM-41 by Modified Thenoyltrifluoroacetone. *Microporous and Mesoporous Materials* **2009**, *120* (3), 317–324. https://doi.org/10.1016/j.micromeso.2008.11.021.

(52) Radi, S.; Abiad, C. E.; Moura, N. M. M.; Faustino, M. A. F.; Neves, M. G. P. M. S. New Hybrid Adsorbent Based on Porphyrin Functionalized Silica for Heavy Metals Removal: Synthesis, Characterization, Isotherms, Kinetics and Thermodynamics Studies. *Journal of Hazardous Materials* **2019**, *370*, 80–90. https://doi.org/10.1016/j.jhazmat.2017.10.058.

(53) Awual, Md. R.; Hasan, Md. M.; Asiri, A. M.; Rahman, M. M. Novel Optical Composite Material for Efficient Vanadium(III) Capturing from Wastewater. *Journal of Molecular Liquids* **2019**, *283*, 704–712. https://doi.org/10.1016/j.molliq.2019.03.119.

(54) Najafi, M.; Yousefi, Y.; Rafati, A. A. Synthesis, Characterization and Adsorption Studies of Several Heavy Metal Ions on Amino-Functionalized Silica Nano Hollow Sphere and Silica Gel. *Separation and Purification Technology* **2012**, *85*, 193–205. https://doi.org/10.1016/j.seppur.2011.10.011.

(55) Langmuir, I. THE CONSTITUTION AND FUNDAMENTAL PROPERTIES OF SOLIDS AND LIQUIDS. PART I. SOLIDS. *J. Am. Chem. Soc.* **1916**, *38* (11), 2221–2295. https://doi.org/10.1021/ja02268a002.

(56) Freundlich, H. Über Die Adsorption in Lösungen. *Zeitschrift für Physikalische Chemie* **1907**, *57U* (1), 385–470. https://doi.org/10.1515/zpch-1907-5723.

(57) Temkin, M. I. Kinetics of Ammonia Synthesis on Promoted Iron Catalysts. *Acta physiochim. URSS* **1940**, *12*, 327–356.

(58) Sips, R. On the Structure of a Catalyst Surface. *The Journal of Chemical Physics* **1948**, *16* (5), 490–495. https://doi.org/10.1063/1.1746922.

(59) Awual, Md. R. An Efficient Composite Material for Selective Lead(II) Monitoring and Removal from Wastewater. *Journal of Environmental Chemical Engineering* **2019**, *7* (3), 103087. https://doi.org/10.1016/j.jece.2019.103087.

(60) Lagergren, S. K. About the Theory of So-Called Adsorption of Soluble Substances. *Sven. Vetenskapsakad. Handingarl* **1898**, *24*, 1–39.

(61) Ho, Y. S.; McKay, G. Pseudo-Second Order Model for Sorption Processes. *Process Biochemistry* **1999**, *34* (5), 451–465. https://doi.org/10.1016/S0032-9592(98)00112-5.

(62) Chien, S. H.; Clayton, W. R. Application of Elovich Equation to the Kinetics of Phosphate Release and Sorption in Soils. *Soil Science Soc of Amer J* **1980**, *44* (2), 265–268. https://doi.org/10.2136/sssaj1980.03615995004400020013x.

(63) Weber, W. J.; Morris, J. C. Kinetics of Adsorption on Carbon from Solution. *J. Sanit. Engrg. Div.* **1963**, *89* (2), 31–59. https://doi.org/10.1061/JSEDAI.0000430.

(64) Zhou, X.; Zhou, X. THE UNIT PROBLEM IN THE THERMODYNAMIC CALCULATION OF ADSORPTION USING THE LANGMUIR EQUATION. *Chemical Engineering Communications* **2014**, *201* (11), 1459–1467. https://doi.org/10.1080/00986445.2013.818541.

(65) Awual, Md. R.; Hasan, Md. M.; Islam, A.; Asiri, A. M.; Rahman, M. M. Optimization of an Innovative Composited Material for Effective Monitoring and Removal of Cobalt(II) from Wastewater. *Journal of Molecular Liquids* **2020**, *298*, 112035. https://doi.org/10.1016/j.molliq.2019.112035.

(66) Da'na, E. Adsorption of Heavy Metals on Functionalized-Mesoporous Silica: A Review. *Microporous and Mesoporous Materials* **2017**, *247*, 145–157. https://doi.org/10.1016/j.micromeso.2017.03.050.

(67) Wang, P.; Du, M.; Zhu, H.; Bao, S.; Yang, T.; Zou, M. Structure Regulation of Silica Nanotubes and Their Adsorption Behaviors for Heavy Metal Ions: pH Effect, Kinetics, Isotherms and Mechanism. *Journal of Hazardous Materials* **2015**, *286*, 533–544. https://doi.org/10.1016/j.jhazmat.2014.12.034.

(68) Abollino, O.; Aceto, M.; Malandrino, M.; Sarzanini, C.; Mentasti, E. Adsorption of Heavy Metals on Na-Montmorillonite. Effect of pH and Organic Substances. *Water Research* **2003**, *37* (7), 1619–1627. https://doi.org/10.1016/S0043-1354(02)00524-9.

(69) Nicholls, D. *Complexes and First-Row Transition Elements*; Macmillan Education UK: London, 1974. https://doi.org/10.1007/978-1-349-02335-6.

(70) Chai, W. S.; Cheun, J. Y.; Kumar, P. S.; Mubashir, M.; Majeed, Z.; Banat, F.; Ho, S.-H.; Show, P. L. A Review on Conventional and Novel Materials towards Heavy Metal Adsorption in

Wastewater Treatment Application. *Journal of Cleaner Production* **2021**, *296*, 126589. https://doi.org/10.1016/j.jclepro.2021.126589.

(71) Abu Rumman, G.; Al-Musawi, T. J.; Sillanpaa, M.; Balarak, D. Adsorption Performance of an Amine-Functionalized MCM–41 Mesoporous Silica Nanoparticle System for Ciprofloxacin Removal. *Environmental Nanotechnology, Monitoring & Management* **2021**, *16*, 100536. https://doi.org/10.1016/j.enmm.2021.100536.

(72) Islam, A.; Teo, S. H.; Taufiq-Yap, Y. H.; Ng, C. H.; Vo, D.-V. N.; Ibrahim, M. L.; Hasan, Md. M.; Khan, M. A. R.; Nur, A. S. M.; Awual, Md. R. Step towards the Sustainable Toxic Dyes Removal and Recycling from Aqueous Solution- A Comprehensive Review. *Resources, Conservation and Recycling* **2021**, *175*, 105849. https://doi.org/10.1016/j.resconrec.2021.105849.

(73) Samuel, M. S.; Shang, M.; Klimchuk, S.; Niu, J. Novel Regenerative Hybrid Composite Adsorbent with Improved Removal Capacity for Lead Ions in Water. *Ind. Eng. Chem. Res.* **2021**, *60* (14), 5124–5132. https://doi.org/10.1021/acs.iecr.0c06277.

(74) Tighadouini, S.; Radi, S.; Bacquet, M.; Degoutin, S.; Zaghrioui, M.; Jodeh, S.; Warad, I. Removal Efficiency of Pb(II), Zn(II), Cd(II) and Cu(II) from Aqueous Solution and Natural Water by Ketoenol–Pyrazole Receptor Functionalized Silica Hybrid Adsorbent. *Separation Science and Technology* **2017**, *52* (4), 608–621. https://doi.org/10.1080/01496395.2016.1262874.

(75) Tighadouini, S.; Radi, S.; El Massaoudi, M.; Lakbaibi, Z.; Ferbinteanu, M.; Garcia, Y. Efficient and Environmentally Friendly Adsorbent Based on β-Ketoenol-Pyrazole-Thiophene for Heavy-Metal Ion Removal from Aquatic Medium: A Combined Experimental and Theoretical Study. *ACS Omega* **2020**, *5* (28), 17324–17336. https://doi.org/10.1021/acsomega.0c01616.

(76) Tighadouini, S.; Radi, S.; Ferbinteanu, M.; Garcia, Y. Highly Selective Removal of Pb(II) by a Pyridylpyrazole-β-Ketoenol Receptor Covalently Bonded onto the Silica Surface. *ACS Omega* **2019**, *4* (2), 3954–3964. https://doi.org/10.1021/acsomega.8b03642.

(77) Trama-Freitas, B.; Freitas, J. C. S.; Martins, R. C.; Gando-Ferreira, L. M.; Quinta-Ferreira, M. E.; Quinta-Ferreira, R. M.; Do Carmo, D. R. A Study of Bio-Hybrid Silsesquioxane/Yeast: Biosorption and Neuronal Toxicity of Lead. *Journal of Biotechnology* **2017**, *264*, 43–50. https://doi.org/10.1016/j.jbiotec.2017.10.015.

(78) Awual, Md. R. Novel Conjugated Hybrid Material for Efficient Lead(II) Capturing from Contaminated Wastewater. *Materials Science and Engineering: C* **2019**, *101*, 686–695. https://doi.org/10.1016/j.msec.2019.04.015.

(79) Liu, Y.; Xu, L.; Liu, J.; Liu, X.; Chen, C.; Li, G.; Meng, Y. Graphene Oxides Cross-Linked with Hyperbranched Polyethylenimines: Preparation, Characterization and Their Potential as Recyclable and Highly Efficient Adsorption Materials for Lead(II) Ions. *Chemical Engineering Journal* **2016**, *285*, 698–708. https://doi.org/10.1016/j.cej.2015.10.047.

(80) Liu, J.; Wang, X. Novel Silica-Based Hybrid Adsorbents: Lead(II) Adsorption Isotherms. *The Scientific World Journal* **2013**, *2013*, 1–6. https://doi.org/10.1155/2013/897159.

(81) Fan, H.-T.; Sun, X.-T.; Zhang, Z.-G.; Li, W.-X. Selective Removal of Lead(II) from Aqueous Solution by an Ion-Imprinted Silica Sorbent Functionalized with Chelating N-Donor Atoms. *J. Chem. Eng. Data* **2014**, *59* (6), 2106–2114. https://doi.org/10.1021/je500328t.

(82) Chen, F.; Wu, Q.; Lü, Q.; Xu, Y.; Yu, Y. Synthesis and Characterization of Bifunctional Mesoporous Silica Adsorbent for Simultaneous Removal of Lead and Nitrate Ions. *Separation and Purification Technology* **2015**, *151*, 225–231. https://doi.org/10.1016/j.seppur.2015.07.024.

(83) Simões, C.; Gomes, M. C.; Neves, M. G. P. M. S.; Cunha, Â.; Tomé, J. P. C.; Tomé, A. C.; Cavaleiro, J. A. S.; Almeida, A.; Faustino, M. A. F. Photodynamic Inactivation of Escherichia Coli with Cationic Meso-Tetraarylporphyrins – The Charge Number and Charge Distribution Effects. *Catalysis Today* **2016**, *266*, 197–204. https://doi.org/10.1016/j.cattod.2015.07.031.